JUN 4 1976

AEDC-TR-76-29

Cy.2

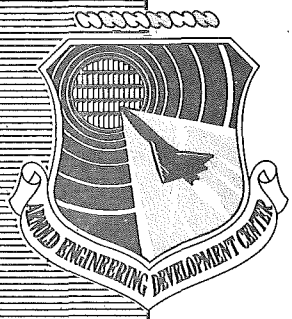

DFVLR/AEDC COOPERATIVE THERMAL VACUUM TEST III

VON KÁRMÁN GAS DYNAMICS FACILITY
ARNOLD ENGINEERING DEVELOPMENT CENTER
AIR FORCE SYSTEMS COMMAND
ARNOLD AIR FORCE STATION, TENNESSEE 37389

May 1976

Final Report for Period 10 February – 30 June, 1975

Approved for public release; distribution unlimited.

Property of U. S. Air Force
AEDC LIBRARY
F40600-75-C-0001

PROPERTY OF U.S. AIR FORCE
AEDC TECHNICAL LIBRARY
ARNOLD AFB, TN 37389

Prepared for

DIRECTORATE OF TECHNOLOGY
ARNOLD ENGINEERING DEVELOPMENT CENTER
ARNOLD AIR FORCE STATION, TENNESSEE 37389

NOTICES

When U. S. Government drawings specifications, or other data are used for any purpose other than a definitely related Government procurement operation, the Government thereby incurs no responsibility nor any obligation whatsoever, and the fact that the Government may have formulated, furnished, or in any way supplied the said drawings, specifications, or other data, is not to be regarded by implication or otherwise, or in any manner licensing the holder or any other person or corporation, or conveying any rights or permission to manufacture, use, or sell any patented invention that may in any way be related thereto.

Qualified users may obtain copies of this report from the Defense Documentation Center.

References to named commercial products in this report are not to be considered in any sense as an endorsement of the product by the United States Air Force or the Government.

This report has been reviewed by the Information Office (OI) and is releasable to the National Technical Information Service (NTIS). At NTIS, it will be available to the general public, including foreign nations.

APPROVAL STATEMENT

This technical report has been reviewed and is approved for publication.

FOR THE COMMANDER

Eules L. Hively

EULES L. HIVELY
Research and Development
Division
Directorate of Technology

Robert O Dietz

ROBERT O. DIETZ
Director of Technology

REPORT DOCUMENTATION PAGE		READ INSTRUCTIONS BEFORE COMPLETING FORM
1. REPORT NUMBER AEDC-TR-76-29	2. GOVT ACCESSION NO.	3. RECIPIENT'S CATALOG NUMBER
4. TITLE *(and Subtitle)* DFVLR/AEDC COOPERATIVE THERMAL VACUUM TEST III		5. TYPE OF REPORT & PERIOD COVERED Final Report, 10 Feb - 30 June 1975 6. PERFORMING ORG. REPORT NUMBER
7. AUTHOR*(s)* W. M. Warmbrod and J. A. Roux, ARO, Inc.		8. CONTRACT OR GRANT NUMBER*(s)*
9. PERFORMING ORGANIZATION NAME AND ADDRESS Arnold Engineering Development Center (DY) Air Force Systems Command Arnold Air Force Station, TN 37389		10. PROGRAM ELEMENT, PROJECT, TASK AREA & WORK UNIT NUMBERS Program Element 65807F
11. CONTROLLING OFFICE NAME AND ADDRESS Directorate of Technology (DYFS) Arnold Engineering Development Center Arnold Air Force Station, TN 37389		12. REPORT DATE May 1976 13. NUMBER OF PAGES 74
14. MONITORING AGENCY NAME & ADDRESS*(if different from Controlling Office)*		15. SECURITY CLASS. *(of this report)* UNCLASSIFIED 15a. DECLASSIFICATION/DOWNGRADING SCHEDULE N/A

16. DISTRIBUTION STATEMENT *(of this Report)*

Approved for public release; distribution unlimited.

17. DISTRIBUTION STATEMENT *(of the abstract entered in Block 20, if different from Report)*

18. SUPPLEMENTARY NOTES

Available in DDC

19. KEY WORDS *(Continue on reverse side if necessary and identify by block number)*

simulators	calibration
space simulation	blackbody radiation
solar simulation	reflectance
temperature measurements	cryopumping

20. ABSTRACT *(Continue on reverse side if necessary and identify by block number)*

A 40-cm-diam sphere and a 30- by 30-cm flat plate, which was used to simulate a hot spot, were tested in the AEDC Aerospace Chamber (12V). This test was part of a cooperative thermal vacuum test program between AEDC and DFVLR in Porz-Wahn, West Germany. The test was conducted in four phases. Phase I was conducted with the solar simulator (radiant flux of one solar constant) and employed both the filtered (spectrally) and

DD FORM 1 JAN 73 1473 EDITION OF 1 NOV 65 IS OBSOLETE

20. ABSTRACT (Continued)

unfiltered modes; the flat plate temperature was fixed at -190, 21, and 125°C. In Phase II the solar simulator was turned off and the temperature about the test sphere was measured for flat plate temperatures of -190, 21, and 125°C. For Phase III the solar simulator was again turned off and small strip heaters were attached to the interior of the hollow test sphere. The heaters were used to simulate hot spots on the sphere, with the heaters set to produce 0.10, 0.25, 0.50, 0.75, and 1.00 watts of heat. The results of this test were compared with some of the results obtained on the same sphere when tested by DFVLR in Porz-Wahn. For Phase IV the infrared (IR) scanning camera was employed to remotely map the temperature of the sphere. The thermocouple results are compared with the IR camera temperature measurements.

AFSC
Arnold AFS Tenn

PREFACE

The work reported herein was conducted by the Arnold Engineering Development Center (AEDC), Air Force Systems Command (AFSC), under Program Element 65807F. The results of the research were obtained by ARO, Inc. (a subsidiary of Sverdrup & Parcel and Associates, Inc.), contract operator of AEDC, AFSC, Arnold Air Force Station, Tennessee, under ARO Project Numbers V32S-69A, V41R-00A, and V41R-01A. The authors of this report were W. M. Warmbrod and J. A. Roux, ARO, Inc. The manuscript (ARO Control No. ARO-VKF-TR-75-106) was submitted for publication on June 30, 1975.

CONTENTS

		Page
1.0	INTRODUCTION	9
2.0	APPARATUS	
	2.1 Test Model	10
	2.2 Test Model Instrumentation	10
	2.3 Test Chamber	17
	2.3.1 Solar Simulator	17
	2.3.2 Cryogenic System	22
	2.4 Chamber Instrumentation	22
	2.5 Infrared Scanning Camera	27
3.0	PROCEDURE	
	3.1 Phase I	28
	3.1.1 Solar Calibration	28
	3.1.2 Test Model Installation	28
	3.1.3 Test Sequence	33
	3.2 Phase II	33
	3.2.1 Test Model Installation	33
	3.2.2 Chamber Configuration	34
	3.2.3 Test Sequence	34
	3.3 Phase III	35
	3.3.1 Test Model Heaters	35
	3.3.2 Test Model Installation	35
	3.3.3 Chamber Configuration	35
	3.3.4 Test Sequence	35
	3.4 Phase IV	37
	3.4.1 Test Model Installation	37
	3.4.2 Thermovision Camera Installation	37
	3.4.3 Chamber Configuration	37
	3.4.4 Test Sequence	37
4.0	RESULTS	
	4.1 Chamber Thermal Environment	38
	4.1.1 Cryosurface Temperatures	38
	4.1.2 Solar Spectral Calibration	40
	4.1.3 Solar Irradiance	41
	4.2 Phase I Results	41
	4.3 Phase II Results	46
	4.4 Phase III Results	46
	4.5 Phase IV Results	62
5.0	CONCLUSIONS	72
	REFERENCES	74

ILLUSTRATIONS

Figure		Page
1.	40-cm-diam Sphere and Flat Plate Mounted in 12V Chamber for Phase I	11
2.	Thermocouple Locations on 40-cm-diam Sphere	15
3.	Thermocouple Locations on 30- by 30-cm Flat Plate	16
4.	Aerospace Chamber 12V	18
5.	Schematic of 12V Solar Simulator	19
6.	Integrating Lens LN_2 Shutter	20
7.	12V Solar Spectrum - Unfiltered	21
8.	12V Solar Spectrum - Filtered	21
9.	Schematic of Chamber Cryosurfaces	23
10.	Map of Solar Irradiance without Filters	29
11.	Map of Solar Irradiance with Filters	30
12.	Sphere Orientation in 12V Chamber	31
13.	Sphere Temperature Distribution for Filtered Solar and -190°C Plate Temperature	42
14.	Sphere Temperature Distribution for Unfiltered Solar and -190°C Plate Temperature	42
15.	Sphere Temperature Distribution for Filtered Solar and 21°C Plate Temperature	43
16.	Sphere Temperature Distribution for Unfiltered Solar and 21°C Plate Temperature	43
17.	Sphere Temperature Distribution for Filtered Solar and 125°C Plate Temperature	44
18.	Sphere Temperature Distribution for Unfiltered Solar and 125°C Plate Temperature	44
19.	Sphere Temperature Distribution via DFVLR with Solar Simulator and No Hot Spot	47

Figure		Page
20.	Transient Response of Surface Thermocouples 1 through 10 with Filtered Solar	48
21.	Transient Response of the Inner Sphere Thermocouple (No. 41) with Filtered Solar	48
22.	Sphere Temperature Distribution for Cold Conditions	49
23.	Sphere Temperature Distribution for 21°C Plate Temperature without Solar Simulation	49
24.	Sphere Temperature Distribution for 125°C Plate Temperature without Solar Simulation	50
25.	DFVLR Results for Sphere Temperature Distribution for 125°C Plate Temperatures without Solar Simulation (Ref. 6)	51
26.	Sphere Temperature Distribution for Cold Equilibrium Condition	53
27.	Sphere Temperature Distribution, Segment 1 Heated with 0.1 w	53
28.	Sphere Temperature Distribution, Segment 1 Heated with 0.25 w	54
29.	Sphere Temperature Distribution, Segment 1 Heated with 0.5 w	54
30.	Sphere Temperature Distribution, Segment 1 Heated with 0.75 w	54
31.	Sphere Temperature Distribution, Segment 1 Heated with 1.0 w	55
32.	Analytical Sphere Temperature Distribution, Segment No. 1 Heated (Ref. 6)	55
33.	Sphere Temperature Distribution, Segment 11 Heated with 0.1 w	57
34.	Sphere Temperature Distribution, Segment 11 Heated with 0.25 w	57
35.	Sphere Temperature Distribution, Segment 11 Heated with 0.5 w	57

Figure		Page
36.	Sphere Temperature Distribution, Segment 11 Heated with 0.75 w	58
37.	Sphere Temperature Distribution, Segment 11 Heated with 1.0 w.	58
38.	Analytical Sphere Temperature Distribution, Segment 11 Heated (Ref. 6)	58
39.	Sphere Temperature Distribution, Segment 11 Heated with 1.0 w and Segment 6 Heated with 0.5 w	59
40.	Sphere Temperature Distribution, Segment 11 Heated with 1.0 w and Segment 16 Heated with 0.5 w	59
41.	Sphere Temperature Distribution, Segment 11 Heated with 1.0 w and Segment 26 Heated with 0.5 w	59
42.	Sphere Temperature Distribution, Segment 11 Heated with 1.0 w and Segment 36 Heated with 0.5 w	60
43.	Analytical Sphere Temperature Distribution, Segment 11 Heated with 1.0 w and Segment 6 Heated with 0.5 w (Ref. 6)	60
44.	Analytical Sphere Temperature Distribution, Segment 11 Heated with 1.0 w and Segment 16 Heated with 0.5 w (Ref. 6)	61
45.	Analytical Sphere Temperature Distribution, Segment 11 Heated with 1.0 w and Segment 26 Heated with 0.5 w (Ref. 6)	61
46.	Analytical Sphere Temperature Distribution, Segment 11 Heated with 1.0 w and Segment 36 Heated with 0.5 w (Ref. 6)	62
47.	Sphere Temperature Distribution under Cold Equilibrium Conditions	62
48.	IR Camera Picture of 27°C Blackbody with Cold Sphere ($T \approx -100°C$) and Solar Simulation (Camera Setting: Sensitivity = 10)	63
49.	IR Camera Picture of 35°C Blackbody with Sphere Heated by Solar Simulator (Camera Setting: Sensitivity = 100)	63

Figure Page

50. IR Camera Picture of 49°C Blackbody with Sphere Heated by Solar Simulator (Camera Setting: Sensitivity = 100) 65

51. IR Camera Picture of 63°C Blackbody with Sphere Heated by Solar Simulator (Camera Setting: Sensitivity = 50) 65

52. IR Camera Picture of 65°C Blackbody with Sphere Heated by Solar Simulator (Camera Setting: Sensitivity = 100) 67

53. IR Camera Picture of 70°C Blackbody with Sphere Heated by Solar Simulator (Camera Setting: Sensitivity = 20) 67

54. IR Camera Picture of 70°C Blackbody with Sphere Heated by Solar Simulator (Camera Setting: Sensitivity = 50) 68

55. IR Camera Picture of 75°C Blackbody with Sphere Heated by Solar Simulator (Camera Setting: Sensitivity = 10) 68

56. IR Camera Picture of 75°C Blackbody with Sphere Heated by Solar Simulator (Camera Setting: Sensitivity = 20) 69

57. IR Camera Picture of 75°C Blackbody with Sphere Heated by Solar Simulator (Camera Setting: Sensitivity = 50) 69

58. IR Camera Picture Showing the Location of Thermocouples Nos. 1, 10, 11, and 20 (see also Fig. 12b) 70

TABLES

1. Chamber 12V Temperature Sensor Locations 24

2. Summary of Test Conditions 34

3. Typical Chamber Cryogenic Surface Temperatures under Cold Conditions with Solar Off 39

Page

4. Typical Chamber Cryogenic Surface Temperatures with Solar On 40

5. Comparison of Theoretical and Measured Results for Phase III 56

6. Comparison of IR Camera Results with Thermocouple Data 71

1.0 INTRODUCTION

The DFVLR/AEDC Cooperative Test Program was initiated in August 1967. The purpose was to improve the understanding and quality of thermal-vacuum simulation techniques at AEDC and DFVLR through mutual cooperation between the two facilities. The results of some of the work performed previously are presented in Refs. 1 through 6.

In some of this previous work, the effects of cryodeposits and uncooled wall sections were studied. The Aerospace Chamber (12V) at AEDC has liquid nitrogen (LN_2)-cooled walls. However, in these past studies there were some wall sections of the 12V which were not cooled to LN_2 temperature (77°K). Presently, the entire 12V chamber walls and floor are LN_2 cooled; the only uncooled portion of the chamber is the collimating mirror. However, the collimating mirror can be blocked off by an LN_2-cooled platform.

The results presented herein are for a thermal balance test, using a 40-cm-diam hollow sphere. The sphere was instrumented with 41 thermocouples; it was divided into 40 surface segments and had one thermocouple located at the sphere center to measure the integral equilibrium temperature. Slots were cut into the sphere to reduce thermal conduction and therefore highlight the sphere circumferential thermal gradients. Also supplied with the sphere was a 30- by 30-cm flat plate used to simulate a hot spot. Selecting a flat plate permits the defining of a standard hot spot for both AEDC and DFVLR space simulation chambers.

The circumferential temperature distribution and integral equilibrium temperature were measured for a variety of test conditions. In the first phase (Phase I) of the test, the temperatures were measured for both a filtered (spectrally) and an unfiltered solar beam (flux of one solar constant while the flat plate temperature was set at -190, 21, and 125°C). In Phase II the temperatures were again measured for the same plate temperature, although without the use of the solar simulator (totally cold chamber). For Phase III small strip heaters were attached to the interior of the sphere to simulate model hot spots from electronic equipment overheating. This was done to determine the effect of a local hot spot upon the circumferential temperature distribution. Where possible, the data recorded in the AEDC test are compared with the data obtained in the DFVLR test.

In an effort to improve the testing techniques at AEDC, an infrared (IR) scanning camera was used to determine sphere temperatures in

Phase IV. Temperature measurements obtained with the IR camera are made remotely and are compared with the thermocouple data. The IR camera used is the AGA Thermovision System® 680/102B. The comparison of results with the camera and thermocouples showed excellent agreement.

2.0 APPARATUS

2.1 TEST MODEL

The test model is a 40-cm-diam sphere, which was designed and fabricated by DFVLR. The sphere is shown in Figs. 1a through d mounted in the 12V chamber along with a 30- by 30-cm flat plate, which is heated to simulate a chamber hot spot. The plate was also supplied by DFVLR. The sphere is made of aluminum with a wall thickness of 0.5 mm. The outside surface is painted black, and the inside surface is left as machined (ϵ = 0.1 to 0.2) to reduce the internal exchange of radiation. The sphere is divided into 40 equal surface elements by 1.0-mm-wide slits to reduce the circumferential conductive heat transfer within the sphere walls. The slits were cut along the equator and 30 deg northern and southern latitude and along 10 meridians, with only 10-mm material left at the crosspoints of the slits.

The flat, heated plate actually consists of an electrofilm heater, rated at 5 w/sq in., sandwiched between two aluminum sheets with the exterior surface facing the sphere painted black. For this test, when the plate was not being heated, it was actively cooled by means of an LN_2-cooled plate clamped directly behind the flat plate.

2.2 TEST MODEL INSTRUMENTATION

The sphere is instrumented with 41 copper-constantan thermocouples, with one centered on the inside surface of each of the 40 surface elements. The remaining thermocouple is mounted within a 5-mm-diam hollow sphere which is suspended in the center of the test sphere and which measures the integral equilibrium temperature of the test sphere. The exterior surface of this inner sphere is also painted black. The numbered locations of the thermocouples are shown in Fig. 2. This numbering system is actually the mirror image of the system shown in Ref. 6 but is the same as the numbering sequence defined by the instrumentation information supplied with the sphere.

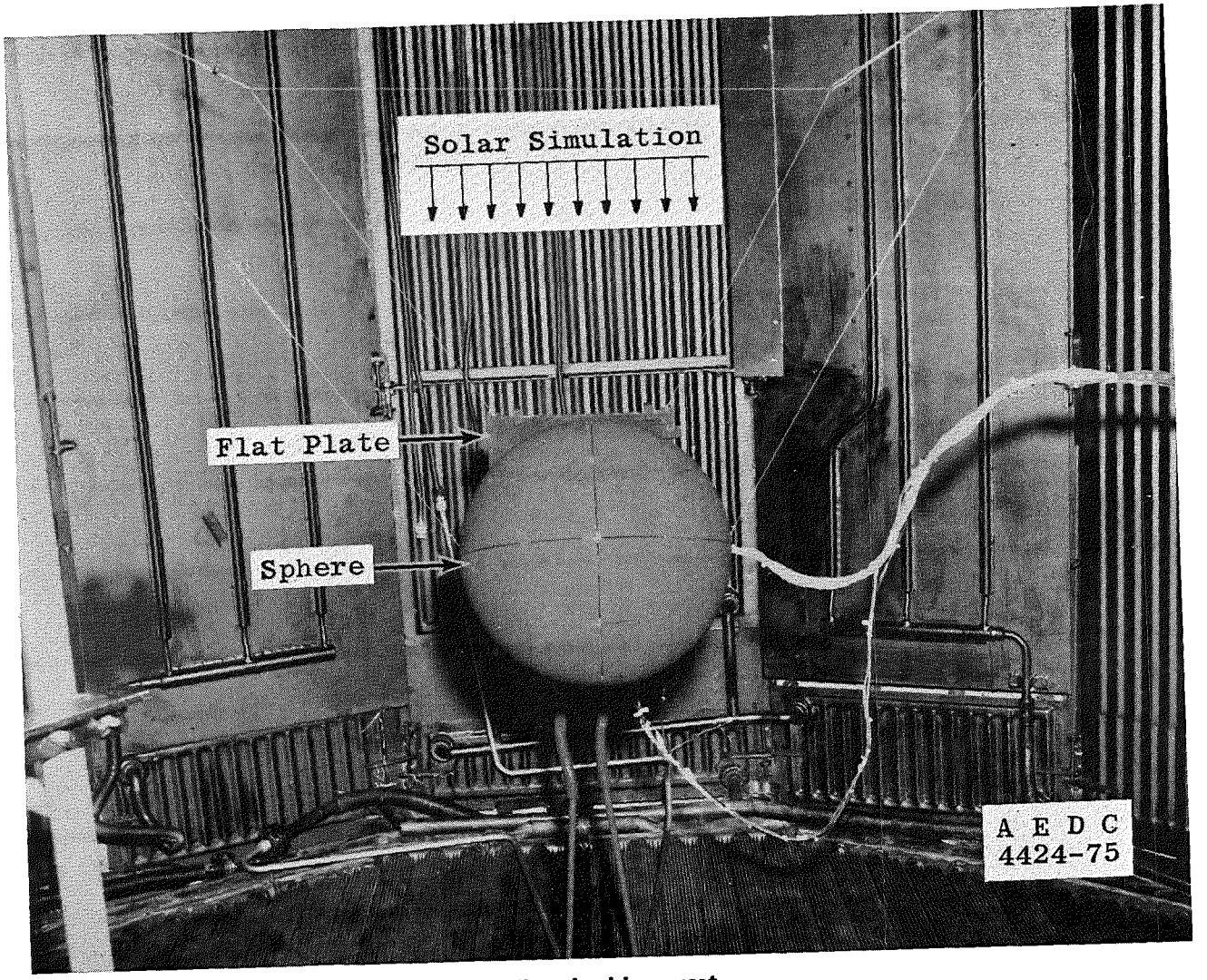

a. View looking west

Figure 1. 40-cm-diam sphere and flat plate mounted in 12V Chamber for Phase I.

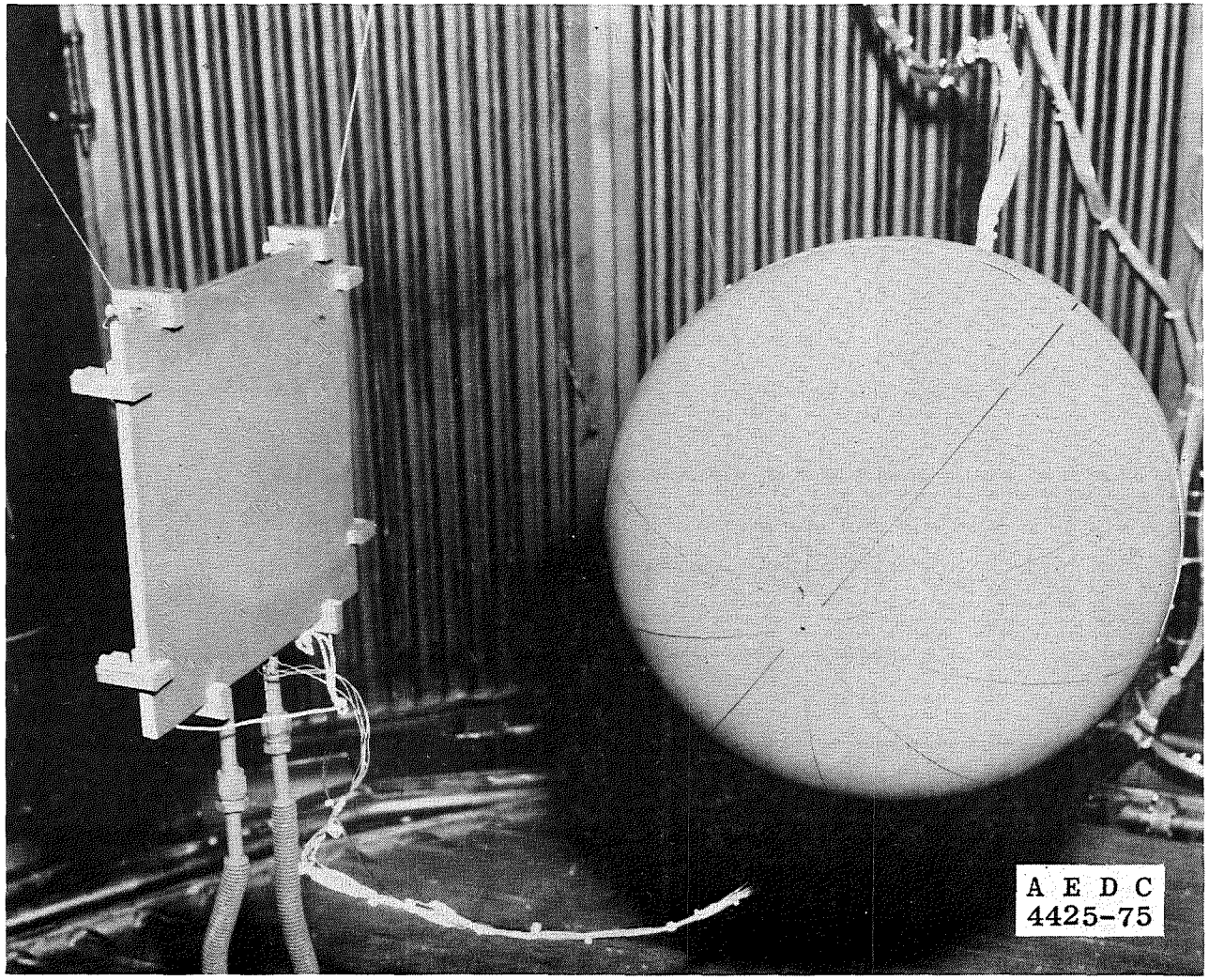

b. View looking north
Figure 1. Continued.

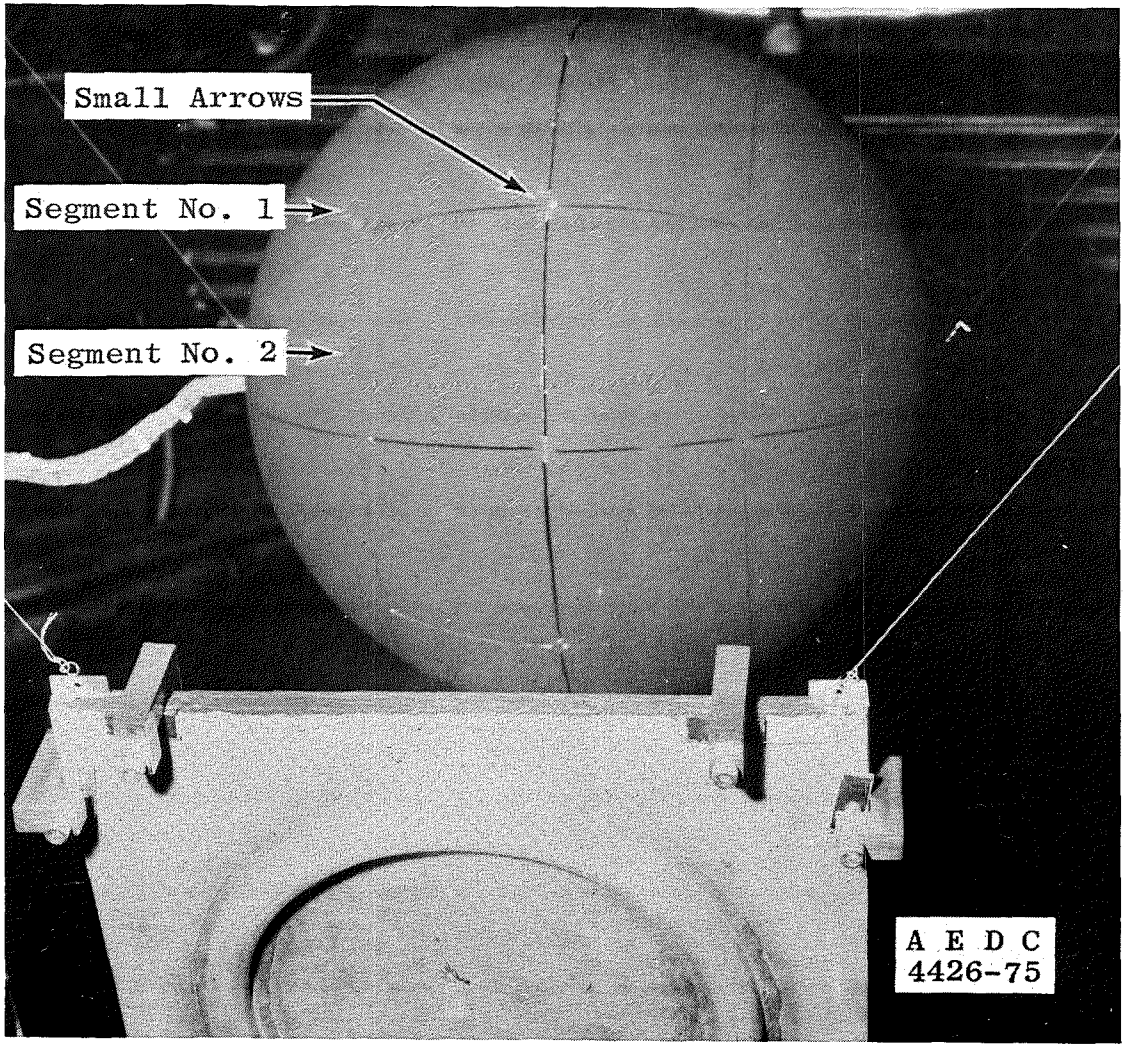

c. View looking east
Figure 1. Continued.

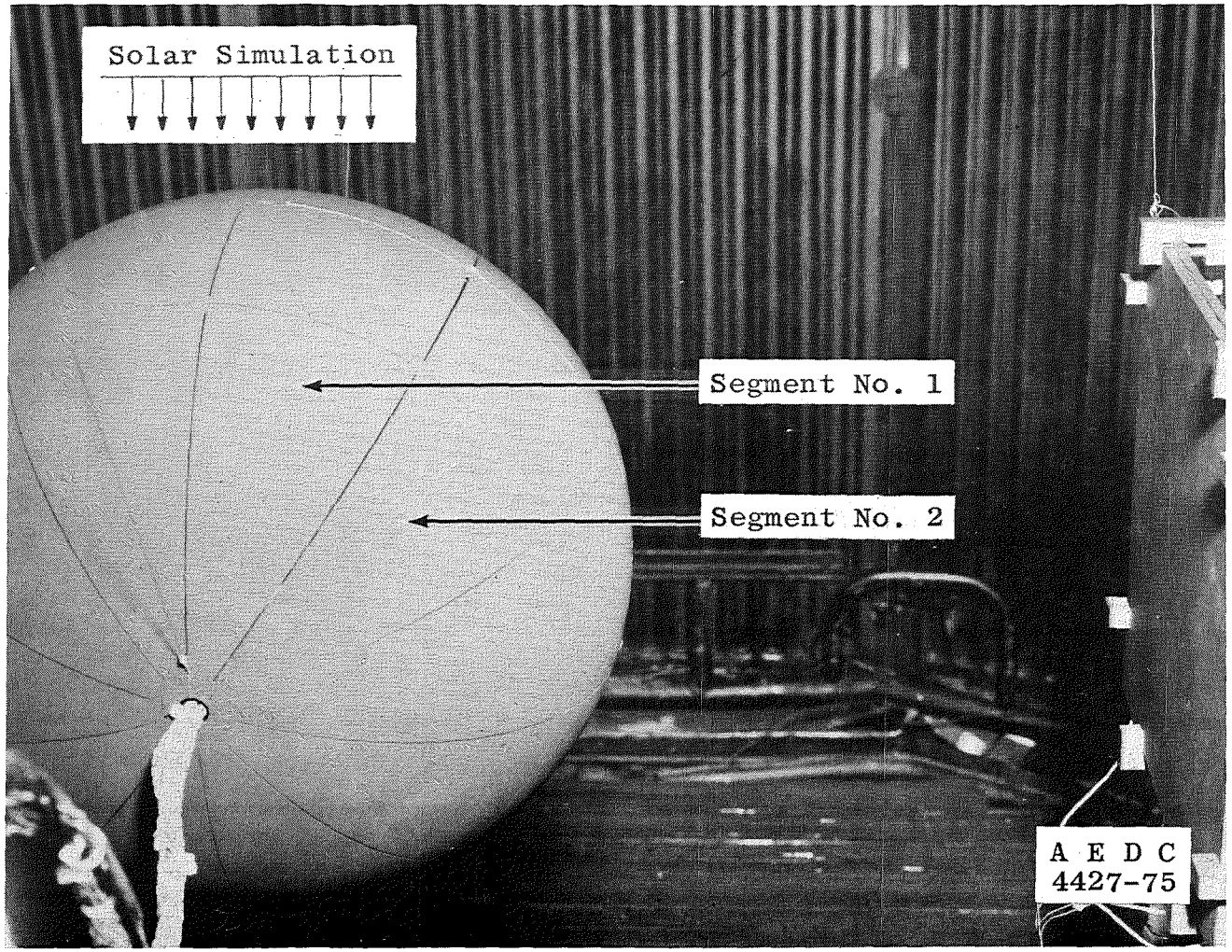

d. View looking south
Figure 1. Concluded.

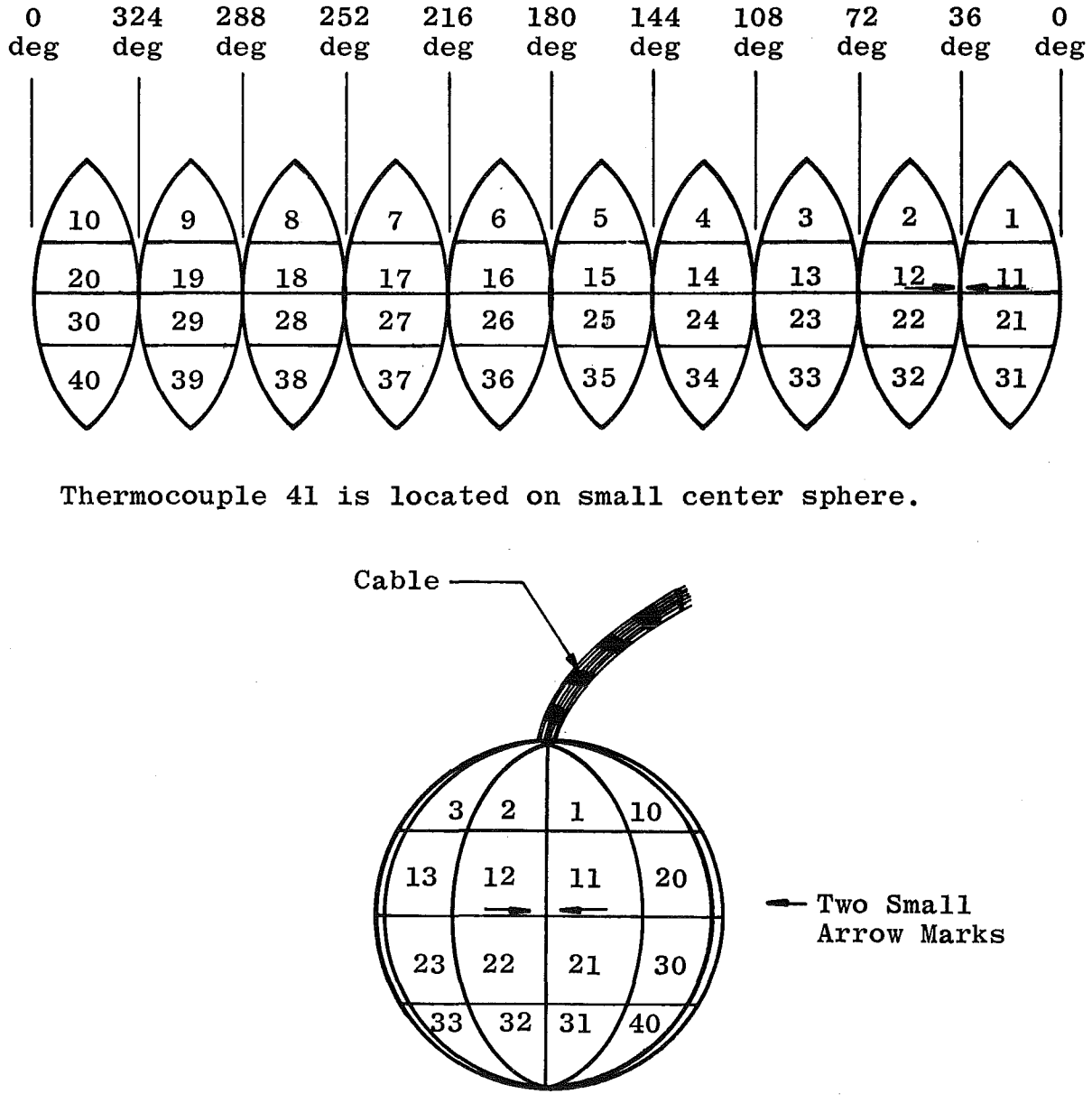

Figure 2. Thermocouple locations on 40-cm-diam sphere.

The flat plate is instrumented with five copper-constantan thermocouples, with the locations shown in Fig. 3. Thermocouple No. 44, which is mounted in the center of the plate, was used to provide a feedback signal to an automatic temperature controller to maintain the preset plate temperature.

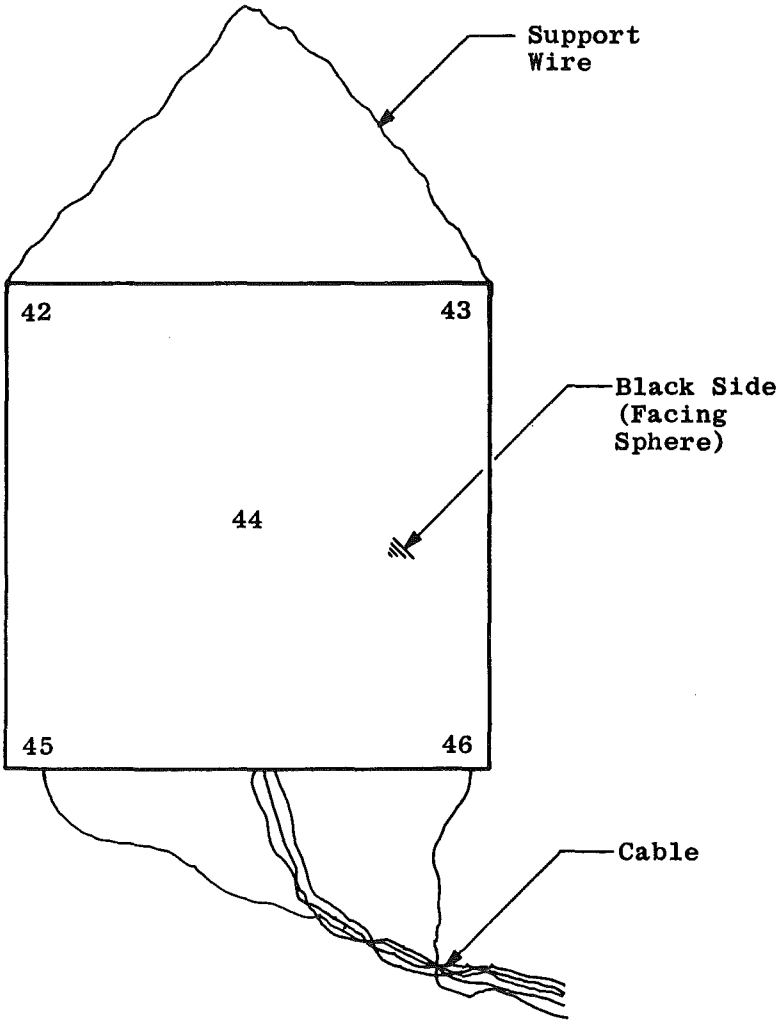

Figure 3. Thermocouple locations on 30- by 30-cm flat plate.

The 46 thermocouples were monitored with the 9300 computer system. The data were processed and printed on line in engineering units and recorded on magnetic tape for later reduction and plotting. During the test, the computer operator was able to select from sample rates of one sample every 15 sec, one sample per minute, and one sample every 5 minutes. Each sample was actually the average of 500 samples taken over a very short time period for each thermocouple. This was done to eliminate the random errors caused by electrical noise. The data reduction for each test condition consisted of time versus temperature plots until equilibrium conditions were reached, and a plot of the equilibrium temperature versus location on the sphere surface.

2.3 TEST CHAMBER

The 12V chamber is a stainless steel vacuum chamber 12 ft in diameter and 35 ft high (Fig. 4). The chamber is lined with a liquid nitrogen (LN_2) cryosurface to simulate the temperature environment of space and contains a working volume approximately 10 ft in diameter by 35 ft high. The top portion of the chamber houses the collimating mirror and entrance window for the off-axis solar simulator. The chamber vacuum pumping system consists of a 750-ft^3/min roughing pump, a 140-ft^3/min forepump, a 750-ft^3/min Roots blower, and a 50,000-ℓ/sec oil diffusion pump.

2.3.1 Solar Simulator

The 12V solar simulator (Fig. 5) is an off-axis system consisting of three basic components: a source lamp array, an integrating lens system, and a collimating mirror. The source is an array of seven 20-kw xenon compact arc lamps in elliptical reflectors. Radiation from the lamp array passes through a quartz integrating lens unit in the chamber wall to a 10-ft-diam aluminized collimating mirror. A water-cooled shutter below the integrating lens is used for off-on cycling of the solar beam. A second shutter, which is LN_2 cooled and is located above the integrating lens (Fig. 6), shields radiant energy emitted by the warm integrating lens from the test volume.

In addition, a spectral filter assembly can be mounted between the source lamp array and the integrating lens system (Fig. 5). The filter arrangement can be varied to filter the radiation of from one to four of the seven xenon lamps.

The solar simulator provides a beam of relatively uniform irradiance (±5 percent) throughout the test volume. Measured beam decollimation is ±2 deg. Spectral distribution of the radiation in the test volume is compared with the Johnson solar distribution in Fig. 7 for the unfiltered solar and in Fig. 8 for the solar with four lamps filtered.

Two LN_2-shielded, water-cooled radiometers are mounted in the test volume to measure the solar beam irradiance during testing. Beam irradiance is adjusted to the desired level by switching on the correct number of lamps and by varying the lamp voltage.

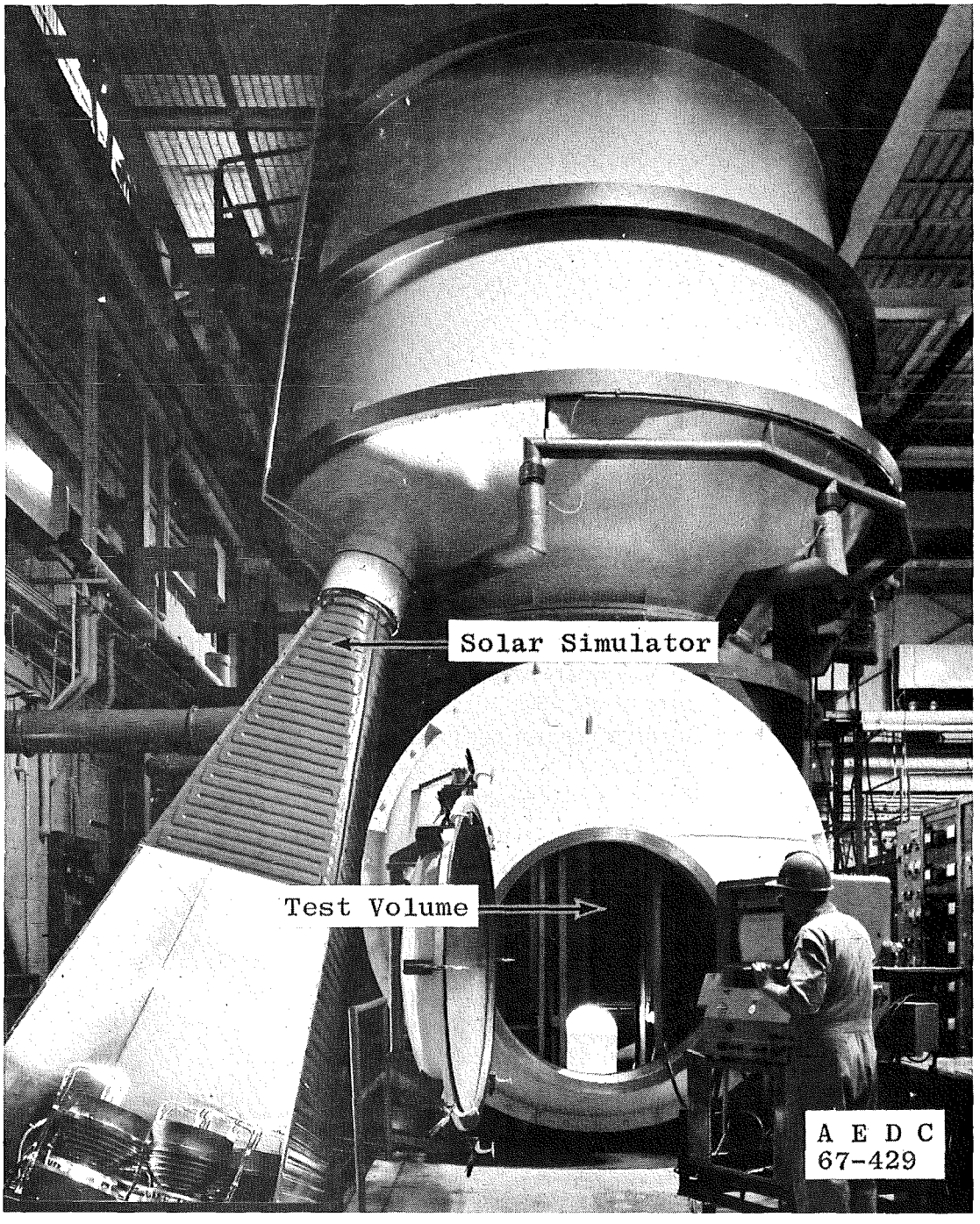

Figure 4. Aerospace Chamber 12V.

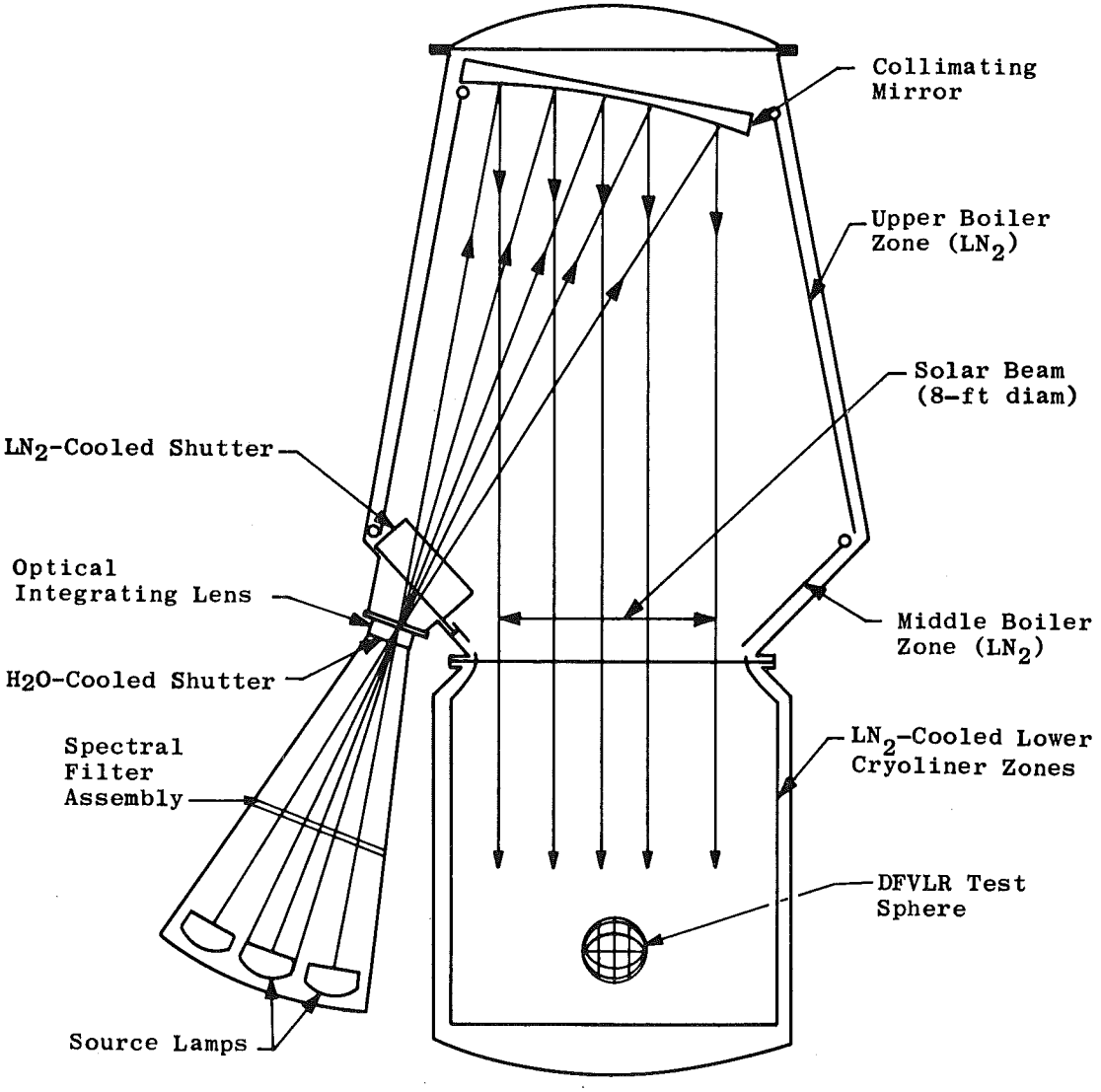

Figure 5. Schematic of 12V solar simulator.

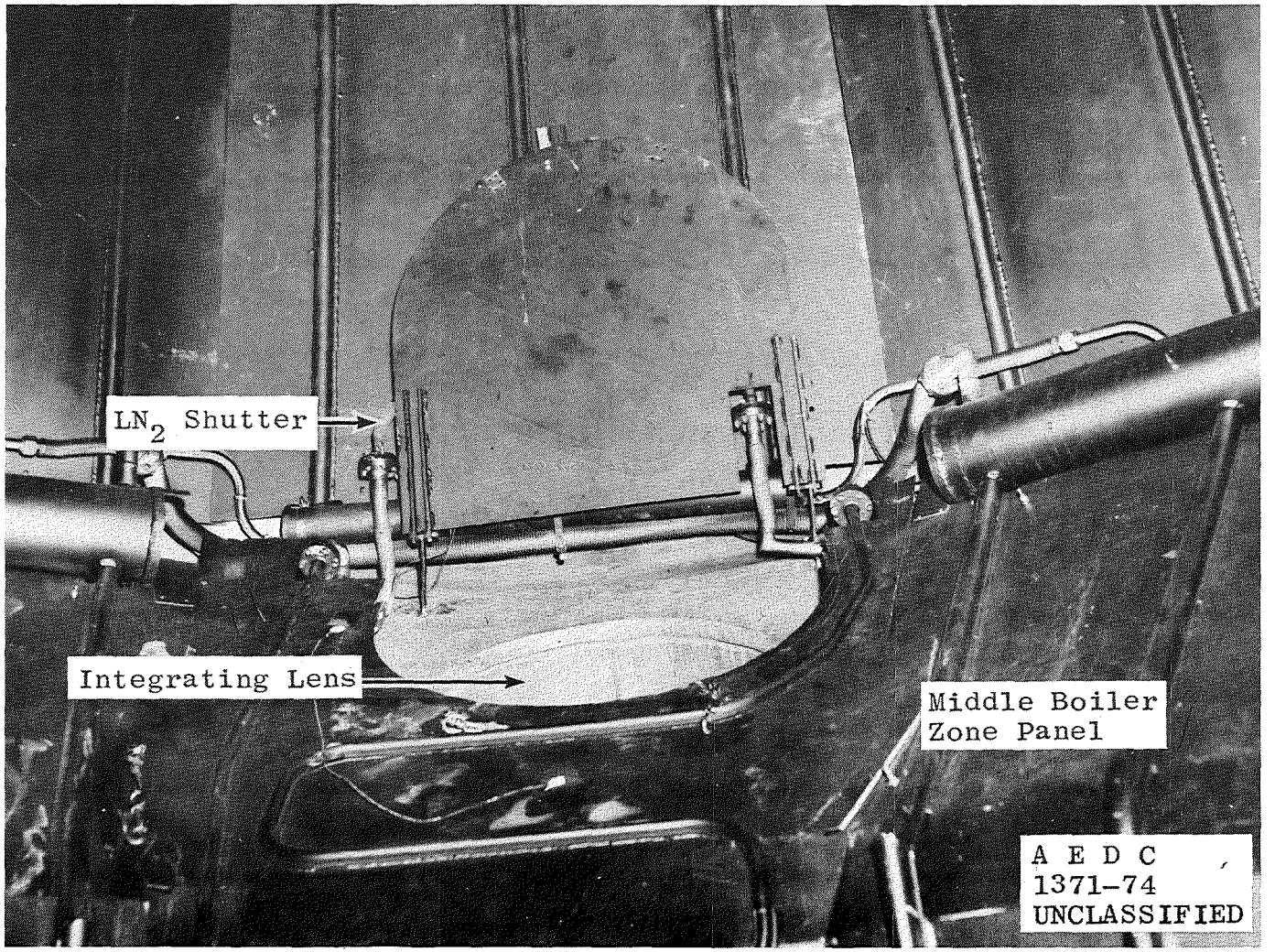

Figure 6. Integrating lens LN_2 shutter.

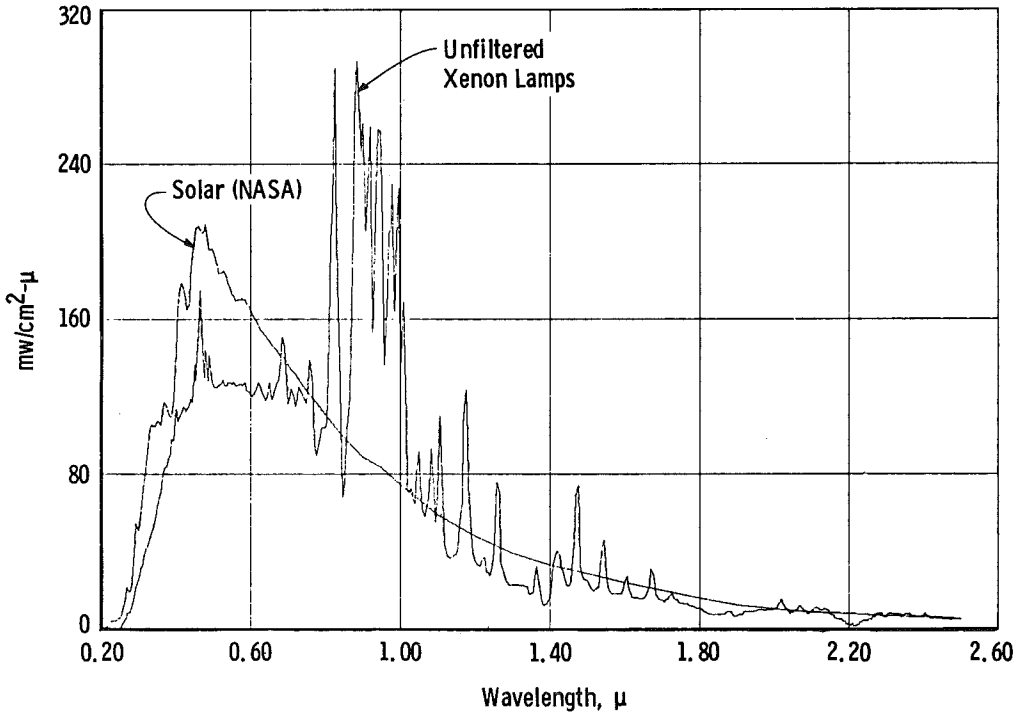

Figure 7. 12V solar spectrum—unfiltered.

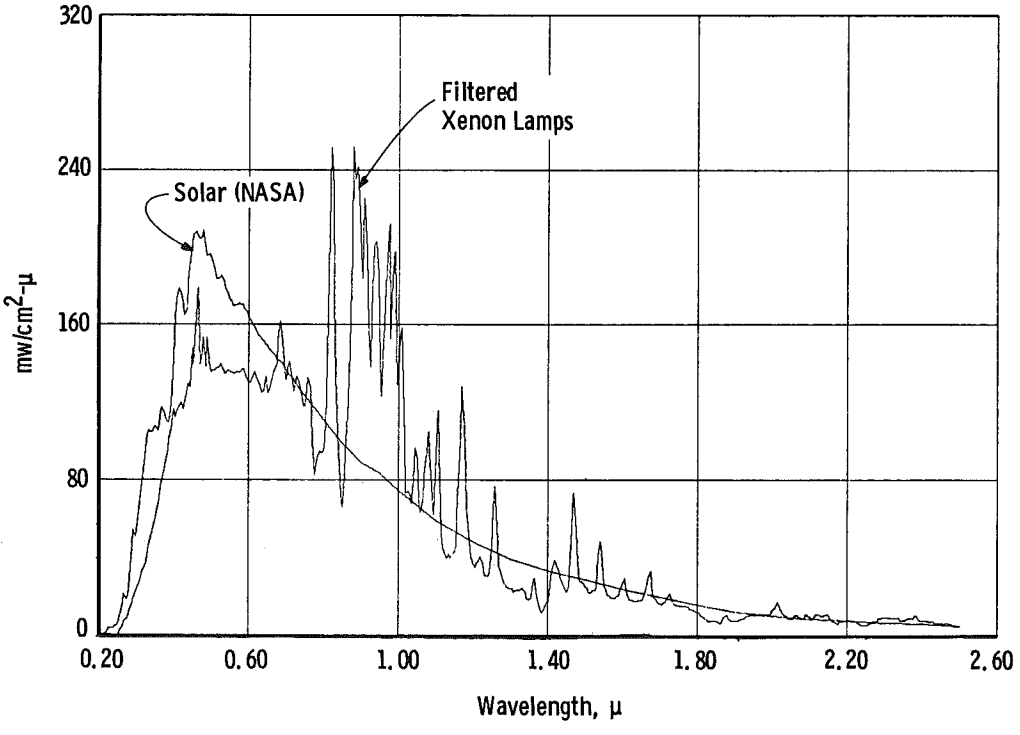

Figure 8. 12V solar spectrum—filtered.

2.3.2 Cryogenic System

The LN_2 cryosurfaces, which completely line the chamber below the solar mirror, simulate the thermal background of space. The LN_2 cryoliner in Chamber 12V is comprised of the upper and middle boiler zones, the lower zone of wall panels which surround the working test volume and which also shield the GHe cryopump, and the deeply grooved high emittance floor panels. Figure 9 is a schematic layout of the chamber wall cryogenic surfaces. Most panels are actively cooled with LN_2 flow from a pressurized LN_2 storage tank, the flow regulated by level controllers in the exhaust lines. Other panels, which comprise only a small fraction of the total panel area, are called filler panels, and these cool by direct thermal contact with the actively cooled panels. The chamber floor, which directly receives the solar beam, is a deeply grooved panel having low reflectance. A small gap at the periphery of the floor panels is covered with an aluminum foil radiation baffle.

The upper portion of the chamber is lined with a single flat cryosurface which parallels the chamber wall. The cryopanels comprise two boiler flow zones, so called because they are cooled by the boiler principle. A LN_2 reservior at the top is partially filled and floods the tubes, which extend to the bottom of the panel. Supply and return flow tubes are concentric; LN_2 from the reservior flows down the inner tube, and a mixture of liquid and vapor, resulting from heat transfer to the outer tube from the cryopanel, flows back to the top of the reservior, where the vapor is vented. Liquid circulation is caused by the difference in pressure head between the liquid vapor mixture in the outer tube and the liquid in the inner tube, and flow is increased as the heat load of the cryosurface is increased. A liquid level controller is used to maintain the liquid level in the reservior. The mirror access platform panels are actively cooled during testing and fold up against the panels of the upper boiler zone.

2.4 CHAMBER INSTRUMENTATION

The LN2 cryosurfaces were instrumented with copper constantan thermocouples. Additional thermocouples provided diagnostic data on the solar simulator. Table 1 lists all the thermocouples installed for the DFVLR program. Approximate locations of thermocouples on the cryosurfaces are shown in Fig. 9. These chamber surface temperatures were monitored and recorded in the range from -210 to 175°C on five multipoint strip chart recorders located in the chamber test control area.

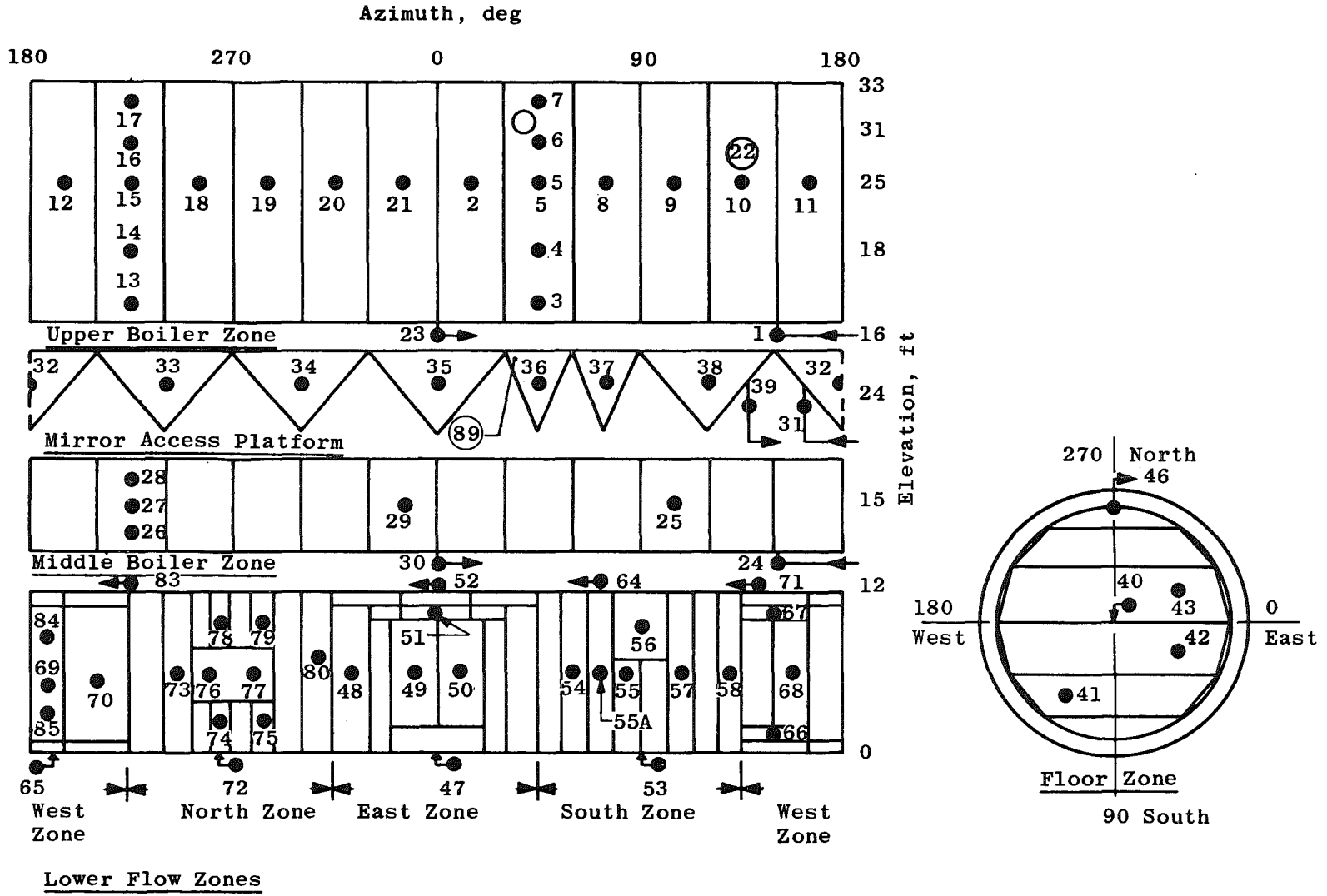

Figure 9. Schematic of chamber cryosurfaces.

Table 1. Chamber 12V Temperature Sensor Locations

LN_2 System Thermocouple Locations

Thermocouple Number	Location
I. Upper Boiler Module Zone	
1	Supply Line - 15 deg
2	Panel, Mid - 15 deg
3	Supply Header - 45 deg
4	Panel, Lower - 45 deg
5	Panel, Mid - 45 deg
6	Panel, Upper - 45 deg
7	Exhaust Header - 45 deg
8	Panel, Mid - 75 deg
9	Panel, Mid - 105 deg
10	Panel, Mid - 135 deg
11	Panel, Mid - 165 deg
12	Panel, Mid - 195 deg
13	Supply Header - 225 deg
14	Panel, Lower - 225 deg
15	Panel, Mid - 225 deg
16	Panel, Upper - 225 deg
17	Exhaust Header - 225 deg
18	Panel, Mid - 255 deg
19	Panel, Mid - 285 deg
20	Panel, Mid - 315 deg
21	Panel, Mid - 345 deg
22	Top Access Plate - 135 deg
23	Exhaust Line - 0 deg
II. Mid Boiler Module Zone	
24	Supply Line - 150 deg
25	Panel, Mid - 105 deg
26	Supply Header - 225 deg
27	Panel, Mid - 225 deg
28	Exhaust Header - 225 deg
29	Panel, Mid - 345 deg
30	Exhaust Line - 0 deg

Table 1. Continued

Thermocouple Number	Location
III. Mirror Inspection Platform	
31	Supply Line - 160 deg
32	Platform - 180 deg
33	Platform - 240 deg
34	Platform - 300 deg
35	Platform - 0 deg
36	Platform - 45 deg
37	Platform - 75 deg
38	Platform - 120 deg
39	Exhaust Line - 140 deg
89	Solar Shield Panel - 45 deg
IV. Floor Zone	
40	Supply Line
41	South Section Fin
43	North Section Fin
46	Exhaust Line
V. East Zone	
47	Supply Line
48	North Active Panel
49	North Door
50	South Door
51	Top Center Panel
52	Exhaust Line - 0 deg
VI. South Zone, Including Integrating Lens Shielding	
53	Supply Line
54	East Tall Panel
55A	Southeast Panel
55	Center Short Panel
56	DP Vane Panel
57	Southwest Panel
58	West Panel
59	Supply Line to Lens Panels, 13 ft, 45 deg
60	Platform Cover Plate, 14 ft, 45 deg

Table 1. Continued

Thermocouple Number	Location
61	Platform Cover Plate, 15 ft, 45 deg
62, 63	Lens Inside Shutter, 15 ft, 45 deg
64	Exhaust Line
VII. West Zone	
65	Supply Line
66	Lower Filler Panel
67	Upper Filler Panel
68	South Tall Panel
69	Mid Tall Panel
70	Hinged Panel
71	Exhaust Line
VIII. North Zone	
72	Supply Line
73	West Tall Panel
74	Lower Northwest Short Panel
75	Lower Northeast Short Panel
76	West Viewport Shield
77	East Viewport Shield
78	Upper Northwest Short Panel
79	Upper Northeast Short Panel
80	East Tall Panel
81	No. 1 Radiometer Shield
82	No. 2 Radiometer Shield
83	Exhaust Line
IX. Scavenger Panel	
84	Panel
85	Panel

Table 1. Concluded

Thermocouple Number	Location
X. Solar Simulation System	
110	Mirror Inspection Platform Support Bracket - 270 deg
111	Solar H_2O Supply
112	Solar H_2O Exhaust
113	Lens Seal - H_2O Exhaust
114	Lens Pebble Plate - H_2O Exhaust
115	Beam House Shutter
116	Beam House Shutter
117	Mirror, North Center
118	Mirror, North Side

The 12V chamber pressure was measured with a Wallace-Tiernan® gage from atmospheric pressure to approximately 10 torr, an MKS Baratron® from 10 to 1 torr, and an NRC® thermocouple gauge between 1 and 1 x 10^{-3} torr. Two NRC ionization gages, one in the bottom and one at the top of the chamber, measured chamber pressure below 1 x 10^{-3} torr; this pressure was recorded on a strip chart.

The solar beam irradiance, as measured by both radiometers, was recorded on strip chart recorders. In addition, one of the radiometers was monitored using the 9300 computer system, with the irradiance data sampled and plotted in the same manner as the test sphere thermocouple data.

2.5 INFRARED SCANNING CAMERA

The IR scanning camera used in this test was the AGA Thermovision System 680/102B, which is equipped with an indium-antimonide (InSb) detector and a 25-deg field-of-view (fov) lens. The InSb detector is sensitive in the 2- to 5-μm wavelength range. In addition, a calibration blackbody, designed and fabricated at AEDC, was used as a reference in the 12V chamber. The blackbody is used as a known blackbody temperature, and all temperature measurements can be made relative

to this known reference. The IR camera was situated to view the test sphere and reference (calibration) blackbody simultaneously from a chamber side viewport. The camera was located approximately 2 m from the sphere and viewed the sphere at about a 30-deg angle from the top. The viewport window was a 5-in.-diam calcium fluoride (CaF_2) window with a transmittance of about 0.93.

3.0 PROCEDURE

3.1 PHASE I

3.1.1 Solar Calibration

A portable radiometer was used to map the solar irradiance over a 2-ft-square area at the centerline of the chamber at the height of the centerline of the test sphere (36 in. above the cryofloor). The solar irradiance was set at approximately one solar constant (135 mw/cm^2), and the two permanently mounted monitor radiometers, which are located at the top of the test volume and near the edge of the beam, were then calibrated based on the average irradiance over the mapped area.

Two calibrations were made, for the unfiltered and filtered configurations. Six lamps were operated for the unfiltered solar, all except lamp No. 7. The measurements were made 6 in. apart over the mapped area for a total of 25 readings, with the results shown in Fig. 10. All seven lamps were operated in the filtered configuration, with the flat circular filters placed in the beams of lamps Nos. 1, 2, 6, and 7. Figure 11 shows the results with filters. The irradiance uniformity was within ±3.5 percent with and without filters over the mapped area.

3.1.2 Test Model Installation

For the first three test phases, the test sphere was mounted 36 in. above the cryofloor in the center of the chamber. The heated plate was mounted vertically, on the west side of the chamber, at a distance of 50 cm from the centerline of the sphere. Both sphere and plate were suspended with stainless steel wire (Fig. 1). Figure 12a shows the orientation of the sphere for Phase I.

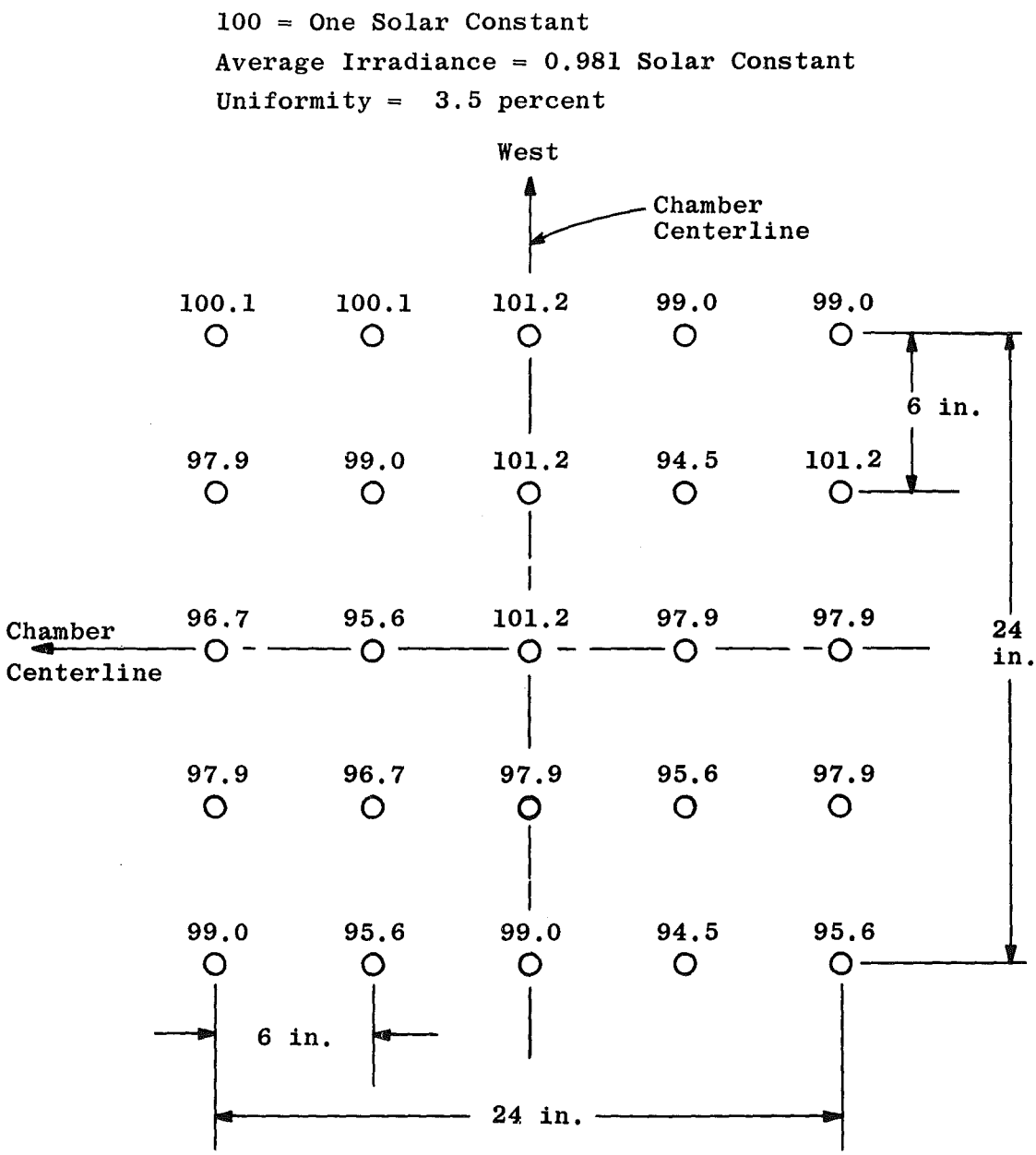

Figure 10. Map of solar irradiance without filters.

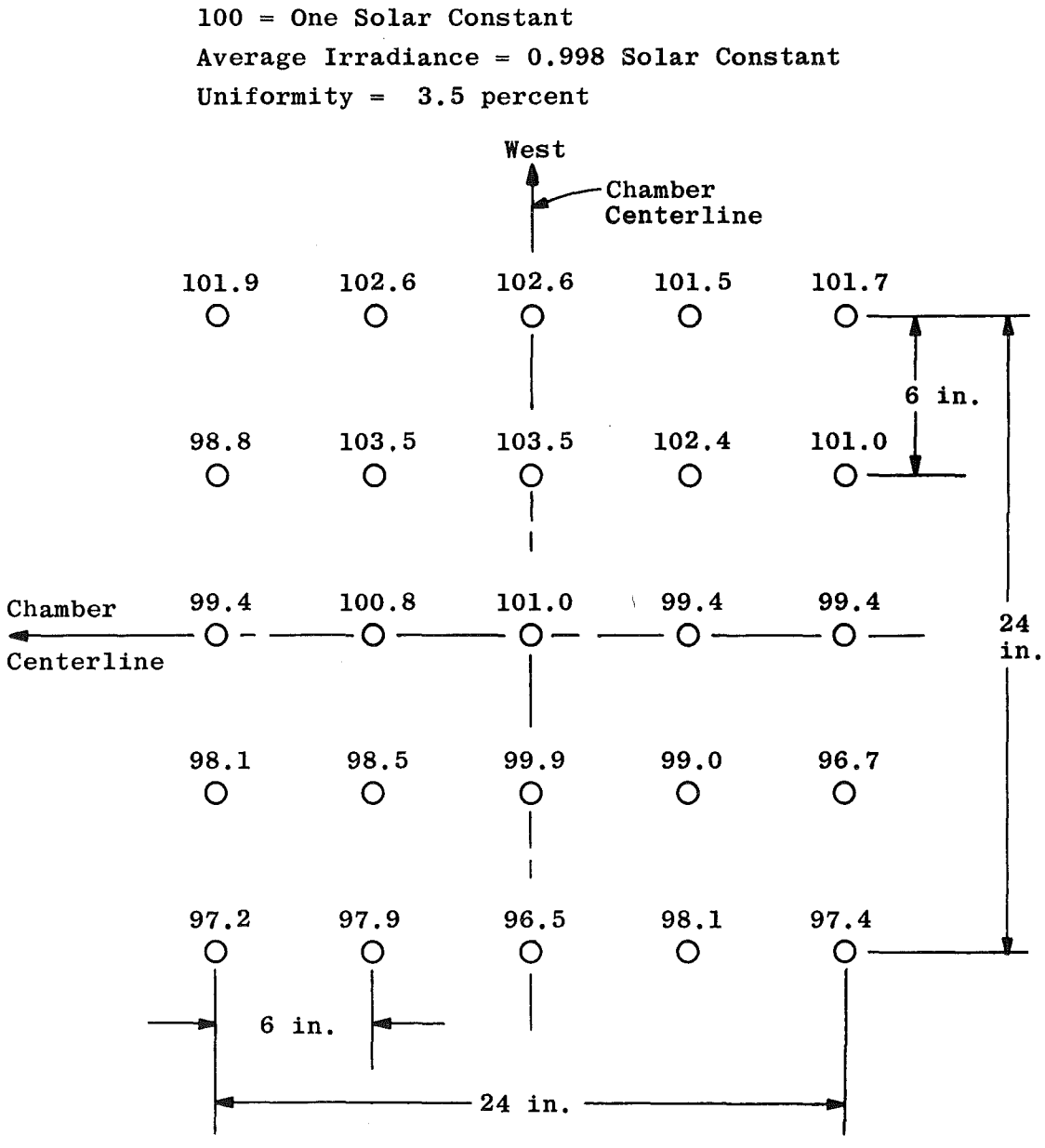

Figure 11. Map of solar irradiance with filters.

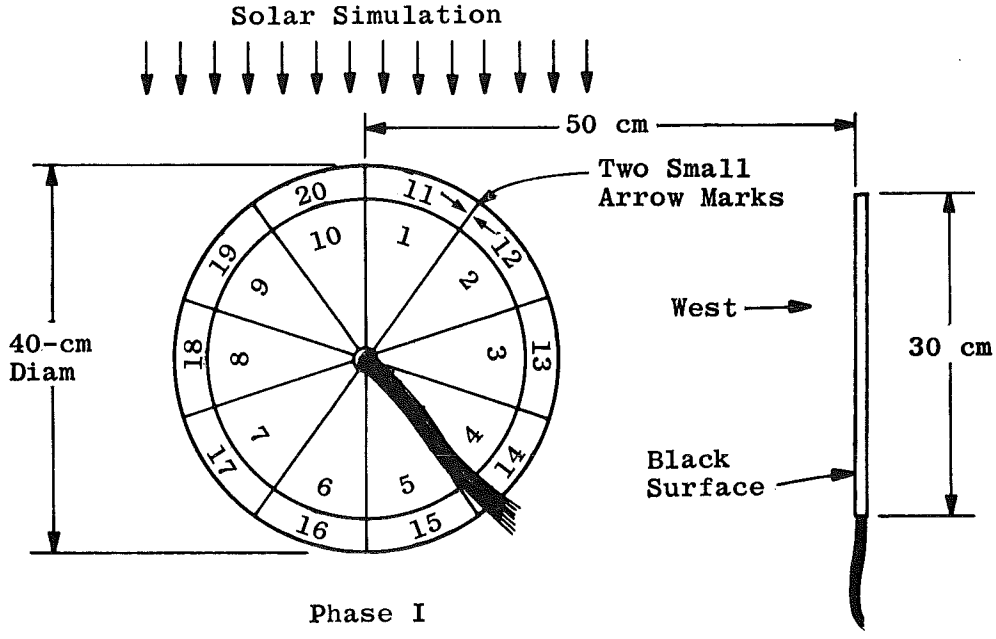

Phase I

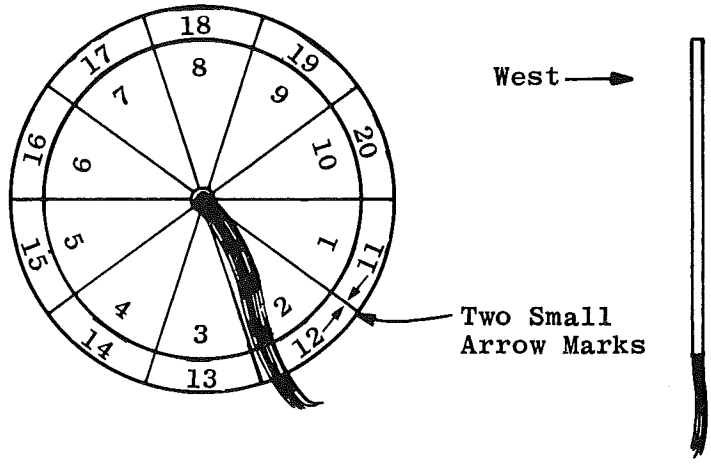

Phase II
Phase III - (Without Flat Plate)

Elevation View Looking South

a. Phases I, II, and III

Figure 12. Sphere orientation in 12V Chamber.

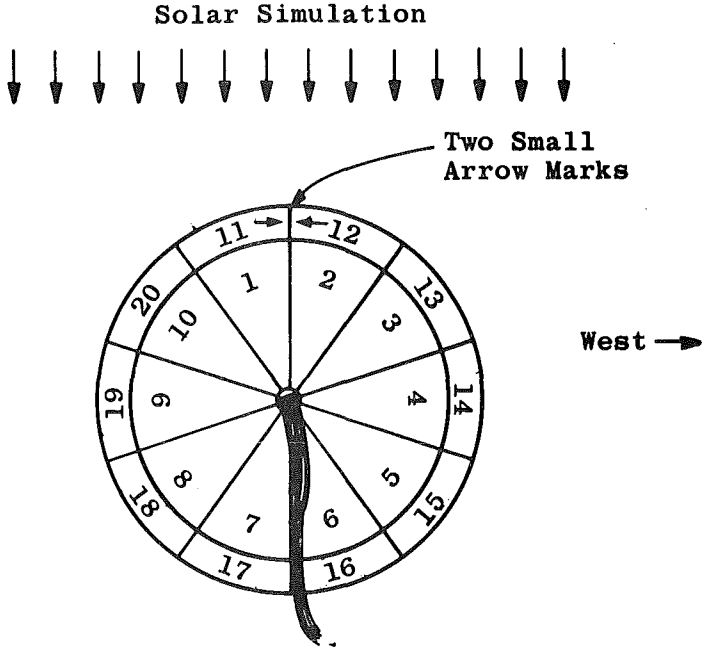

Elevation View
Looking South

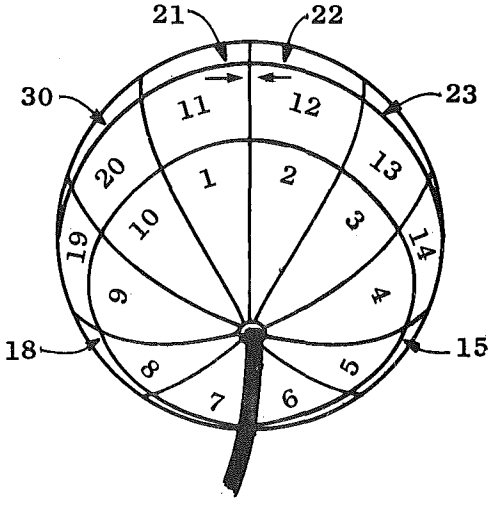

Sphere As Seen with
Thermovision Camera

b. Phase IV
Figure 12. Concluded.

3.1.3 Test Sequence

A summary of the test conditions is presented in Table 2. The procedure used for the Phase I test was as follows:

1. Calibrate and check out the data system.
2. Close access door and evacuate chamber.
3. Cool LN_2 cryosurfaces, including flat plate.
4. Test Run 1020: turn filtered solar on (one solar constant); monitor temperatures until equilibrium conditions are reached.
5. Test Run 1030: with filtered solar on, heat flat plate to 21°C; monitor temperatures until equilibrium conditions are reached.
6. Test Run 1040: with filtered solar on, heat flat plate to 125°C; monitor temperatures until equilibrium conditions are reached.
7. Turn solar and flat plate heater off.
8. Remove spectral filters.
9. Test Run 1070: turn unfiltered solar on (one solar constant); monitor temperatures until equilibrium conditions are reached.
10. Test Run 1050: with unfiltered solar on (one solar constant), heat flat plate to 21°C; monitor temperatures until equilibrium conditions are reached.
11. Test Run 1060: with solar on, heat flat plate to 125°C, monitor temperatures until equilibrium conditions are reached.
12. Turn solar and flat plate heater off.
13. Warm up and repressurize chamber.

3.2 PHASE II

3.2.1 Test Model Installation

For Phase II, the test sphere was rotated 90 deg to obtain the orientation shown in Fig. 12a. This was done to expose the same surface to the flat plate radiation as was exposed to the solar radiation in Phase I.

Table 2. Summary of Test Conditions

Phase	Test Run	LN_2 Cryo-Surfaces	Solar Shutter	Solar Lamps	Flat Plate	Sphere Segments, w					
						1	11	6	16	26	36
I	1020	Cold	Open	Filtered	Cold						
	1030	Cold	Open	Filtered	21°C						
	1040	Cold	Open	Filtered	125°C						
	1070	Cold	Open	Unfiltered	Cold						
	1050	Cold	Open	Unfiltered	21°C						
	1060	Cold	Open	Unfiltered	125°C						
II	2010	Cold	Closed	Off	Cold						
	2020	Cold	Closed	Off	21°C						
	2033	Cold	Closed	Off	125°C						
III	3009	Cold	Closed	Off	Removed						
	3010	Cold	Closed	Off	Removed	0.1					
	3020	Cold	Closed	Off	Removed	0.25					
	3030	Cold	Closed	Off	Removed	0.5					
	3040	Cold	Closed	Off	Removed	0.75					
	3050	Cold	Closed	Off	Removed	1.0					
	3110	Cold	Closed	Off	Removed		1.0	0.5			
	3120	Cold	Closed	Off	Removed		1.0		0.5		
	3059	Cold	Closed	Off	Removed						
	3060	Cold	Closed	Off	Removed		0.1				
	3070	Cold	Closed	Off	Removed		0.25				
	3080	Cold	Closed	Off	Removed		0.5				
	3090	Cold	Closed	Off	Removed		0.75				
	3100	Cold	Closed	Off	Removed		1.0				
	3130	Cold	Closed	Off	Removed		1.0			0.5	
	3140	Cold	Closed	Off	Removed		1.0				0.5
IV	4010	Cold	Open	Filtered	Removed						
	4030	Cold	Open	Filtered	Removed	2.5					

3.2.2 Chamber Configuration

The mirror inspection platform, which is LN_2 cooled, was lowered to shield the sphere from the warm mirror surface during Phase II. The solar remained off and the solar shutters remained closed during Phase II.

3.2.3 Test Sequence

The procedure used for the Phase II test was as follows:

1. Check out data system.
2. Close access door and evacuate chamber.
3. Cool LN_2 cryosurfaces, including flat plate.
4. Test Run 2010: conduct at equilibrium under cold conditions.

5. Test Run 2020: heat flat plate to 21°C; monitor temperatures until equilibrium conditions are reached.
6. Test Run 2033: heat flat plate to 125°C; monitor temperatures until equilibrium conditions are reached.
7. Turn flat plate off.
8. Warm up and repressurize chamber.

3.3 PHASE III

3.3.1 Test Model Heaters

The sphere and flat plate were removed from the chamber, and small Minco Thermofoil® heaters were mounted inside the sphere as follows: heater design "B" for segments 11, 16, and 26, and heater design "N" for segments 1, 6, and 36. Two heaters were arranged symmetrically inside each segment and connected in series. Each "B" heater has a surface area of 1.2 sq in. and a resistance of 80 ohms. Each "N" heater has a surface area of 1.87 sq in. and a resistance of 120 ohms.

3.3.2 Test Model Installation

The sphere was relocated in the chamber as in the previous tests and was oriented as shown in Fig. 12a. The flat plate was not installed for this phase.

3.3.3 Chamber Configuration

The solar remained off, the solar shutters remained closed, and the mirror inspection platform remained lowered for Phase III.

3.3.4 Test Sequence

The procedure used for the Phase III test was as follows:

1. Check out data system.
2. Close access door and evacuate chamber.
3. Cool LN_2 cryosurfaces.

4. Test Run 3009: conduct at equilibrium under cold conditions.
5. Test Run 3010: heat segment 1 with 0.1 w; monitor temperatures until equilibrium conditions are reached.
6. Test Run 3020: repeat with 0.25 w.
7. Test Run 3030: repeat with 0.5 w.
8. Test Run 3040: repeat with 0.75 w.
9. Test Run 3050: repeat with 1.0 w.
10. Turn segment 1 heater off; cool to equilibrium.
11. Test Run 3110: heat segment 11 with 1.0 w and segment 6 with 0.5 w; monitor temperatures until equilibrium conditions are reached.
12. Turn segment 6 heater off; allow to cool.
13. Test Run 3120: with segment 11 heated with 1.0 w, heat segment 16 with 0.5 w; monitor temperatures until equilibrium conditions are reached.
14. Turn segment 11 and 16 heaters off; cool to equilibrium.
15. Test Run 3059: conduct at equilibrium under cold conditions.
16. Test Run 3060: heat segment 11 with 0.1 w; monitor temperatures until equilibrium conditions are reached.
17. Test Run 3070: repeat with 0.25 w.
18. Test Run 3080: repeat with 0.50 w.
19. Test Run 3090: repeat with 0.75 w.
20. Test Run 3100: repeat with 1.0 w.
21. Test Run 3130: with segment 11 heated to 1.0 w, heat segment 26 with 0.5 w; monitor temperatures until equilibrium conditions are reached.

22. Turn segment 26 heater off; allow to cool.
23. Test Run 3140: with segment 11 heated to 1.0 w, heat segment 36 with 0.5 w; monitor temperatures until equilibrium conditions are reached.
24. Turn segment 11 and 16 heaters off.
25. Warm up and repressurize chamber.

3.4 PHASE IV

3.4.1 Test Model Installation

For Phase IV, the test sphere orientation is shown in Fig. 12b. The sphere was raised and shifted off center, toward the north chamber wall, to provide the optimum view for the Thermovision camera. The flat plate was not installed in the chamber for Phase IV.

3.4.2 Thermovision Camera Installation

The Thermovision camera was mounted on a tripod outside the lower viewport on the north chamber wall. The camera axis was inclined downward at a 30-deg angle to the horizontal to provide a view of the top surface of the sphere, where the solar simulation has maximum effect. The black calibration body for the camera was mounted below and behind the sphere, close to the cryofloor. The calibration temperature was adjusted as required during Phase IV.

3.4.3 Chamber Configuration

The mirror inspection platform was raised for Phase IV.

3.4.4 Test Sequence

The Phase IV test procedures were as follows:

1. Calibrate and check out data system.
2. Check out Thermovision camera.
3. Close access door and evacuate chamber.
4. Cool LN_2 cryosurfaces.
5. Warm black calibration body to 30°C.

6. Test Run 4010: turn filtered solar on (one solar constant); monitor temperatures with thermocouples and Thermovision camera until equilibrium temperatures are reached, taking photographs of Thermovision camera results at appropriate intervals.
7. Test Run 4030: with filtered solar on, heat segment 1 with 2.5 w; monitor temperatures with thermocouples and Thermovision camera until equilibrium conditions are reached.
8. Turn segment 1 heater off.
9. Turn solar off.
10. Warm up and repressurize chamber.

4.0 RESULTS

Since the present test was conducted in various phases, the results will be presented in accordance with the different phases of the test. In the data which are presented next, the results from thermocouple 34 are erroneous for Phases I and II. Evidently, the leads from this thermocouple were shorted together at a connection point within the chamber and thus yielded incorrect information. In addition, the results of thermocouple 7 are erroneous for Runs 2020 and 2030 in Phase II because of a bad amplifier. One should keep this in mind when considering the following results.

For all phases, the chamber pressure was maintained between 4.4×10^{-6} and 4.6×10^{-6} torr.

4.1 CHAMBER THERMAL ENVIRONMENT

4.1.1 Cryosurface Temperatures

Chamber cryogenic surface temperatures, as measured by the thermocouples shown in Fig. 9 and listed in Table 1, are recorded in Tables 3 and 4. Table 3 records the temperatures at the time of Run 1010 with all the cryosurfaces cold and with the solar off. Table 4 records the temperatures during Run 1040 with the cryosurfaces cold,

solar on, and the flat plate at 125°C. Temperatures of the cryosurfaces varied only slightly from these distributions during the solar off and solar on test periods. Cryosurface thermocouples 22, 24, 33, 35, 40, and 65 were not reading properly and are omitted from Tables 3 and 4. The following cryosurface thermocouples were not used for this test: 42, 44, 66, 67, 86, 87, 88, and 90 through 109.

Table 3. Typical Chamber Cryogenic Surface Temperatures under Cold Conditions with Solar Off

TC No.	Temp., °C	TC No.	Temp., °C	TC No.	Temp., °C
1	-196	32	-196	68	-196
2	-190			69	-181
3	-196	34	-196	70	-196
4	-190			71	-196
5	-190	36	-196	72	-196
6	-196	37	-196	73	-196
7	-196	38	-196	74	-196
8	-190	39	-196	75	-196
9	-190	41	-196	76	-196
10	-190	43	-196	77	-196
11	-190	46	-196	78	-196
12	-190	47	-196	79	-196
13	-196	48	-196	80	-196
14	-196	49	-171	81	-196
15	-190	50	-171	82	-196
16	-196	51	-196	83	-196
17	-196	52	-196	84	-196
18	-190	53	-190	85	-196
19	-190	54	-190	89	-196
20	-190	55A	-190	110	+ 29
21	-190	55	-190	111	+ 27
23	-196	57	-196	112	+ 27
25	-196	58	-196	113	+ 29
26	-196	59	-196	114	+ 24
27	-196	60	-196	115	+ 27
28	-196	61	-196	116	+ 27
29	-196	62	-196	117	+ 27
30	-196	63	-196	118	+ 21
31	-196	64	-196		

Table 4. Typical Chamber Cryogenic Surface Temperatures with Solar On*

TC No.	Temp., °C	TC No.	Temp., °C	TC No.	Temp., °C
1	-196	32	-196	68	-184
2	-190	34	-196	69	-184
3	-196	36	-196	70	-196
4	-196	37	-196	71	-196
5	-196	38	-196	72	-184
6	-190	39	-196	73	-196
7	-190	41	-196	74	-196
8	-190	43	-196	75	-196
9	-190	46	-196	76	-196
10	-190	47	-196	77	-190
11	-196	48	-196	78	-196
12	-196	49	-171	79	-196
13	-190	50	-171	80	-196
14	-196	51	-190	81	-196
15	-196	52	-190	82	-196
16	-190	53	-190	83	-190
17	-196	54	-196	84	-190
18	-196	55A	-196	85	-190
19	-190	55	-196	89	-190
20	-179	56	-196	110	+ 38
21	-196	57	-196	111	+ 27
23	-190	58	-196	112	+ 32
25	-196	59	-196	113	+ 29
26	-196	60	-196	114	+ 27
27	-190	61	-196	115	+ 27
28	-196	62	-196	116	+ 27
29	-196	63	-190	117	+ 38
30	-196	64	-190	118	+ 32
31	-196				

*Flat Plate Temperature = 125°C

4.1.2 Solar Spectral Calibration

After the test was conducted, a spectral calibration of the solar beam was performed. The solar beam was spectrally scanned, both filtered and unfiltered (spectrally). Spectral filters have been added

to the solar simulator in an effort to produce a solar spectrum which is more nearly like the Johnson curve. This test provided a means for calibrating the filtered solar beam and also for comparing the effects of spectral distribution (one solar constant) upon the sphere temperatures. Shown in Fig. 7 is the spectral distribution of the unfiltered solar; the total flux to the monitoring radiometer was 1.0 solar constant. In Fig. 8 the spectral distribution is shown for the filtered solar beam: for the filtered solar beam the total radiant flux to the monitoring radiometer was 1.0 solar constant. Thus, in Phase I of the test, these are the typical spectral distributions present in the 12 V chamber test section. A comparison of the two curves shows that the filters significantly reduce the xenon peak at 0.9 μ. With the filters, the lamp voltage is increased to produce one solar constant, with a resulting increase in the UV portion of the spectral curve.

4.1.3 Solar Irradiance

The radiant flux levels were set at approximately one solar constant (135 mw/cm^2) for Phase I. The measured flux levels actually varied from 0.965 to 1.010 solar constant (4.5 percent) during the test periods, with a variation of up to 3 percent measured during the individual test runs. Evidently, fluctuations in the line voltage to the lamp power supplies result in the measured fluctuations of the solar flux.

4.2 PHASE I RESULTS

As mentioned earlier, Phase I consisted of measuring the sphere temperature distribution for both the filtered and the unfiltered solar beam, and also for the flat plate temperature taken as -190°C, 21°C, and 125°C. Also, for reviewing the results in this section please note the sphere orientation in Fig. 12a. Figures 13 and 14 show a comparison of the results obtained for a plate temperature of -190°C and for the filtered and unfiltered solar beams, respectively. The integral equilibrium temperature is seen to be slightly higher for the filtered case as opposed to the unfiltered case; also, the temperatures for the other thermocouples are seen to be slightly higher for the filtered case. Figures 15 and 16 show the sphere temperature distribution for a plate temperature of 21°C, again with the solar filtered and unfiltered, respectively. Here, it is seen that again the integral equilibrium temperature for the filtered case is slightly higher than that for the unfiltered case. Similarly, the temperatures measured on the sphere for the filtered case are slightly higher. The results in Figs. 17 and 18 show the data for a flat plate temperature of 125°C with the solar

beam again filtered and unfiltered, respectively. As before, the integral equilibrium temperature and sphere temperatures are slightly higher for the filtered case. It is felt that the temperatures for the unfiltered case are lower because of a slightly lower flux reading on the monitoring radiometer rather than due to the spectral redistribution of the solar beam.

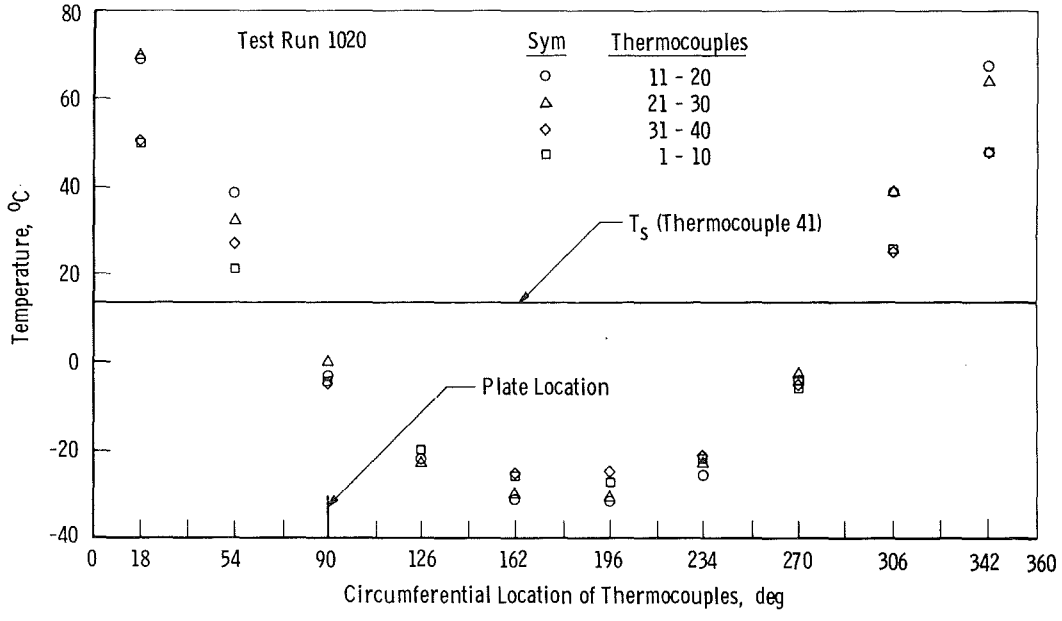

Figure 13. Sphere temperature distribution for filtered solar and -190°C plate temperature.

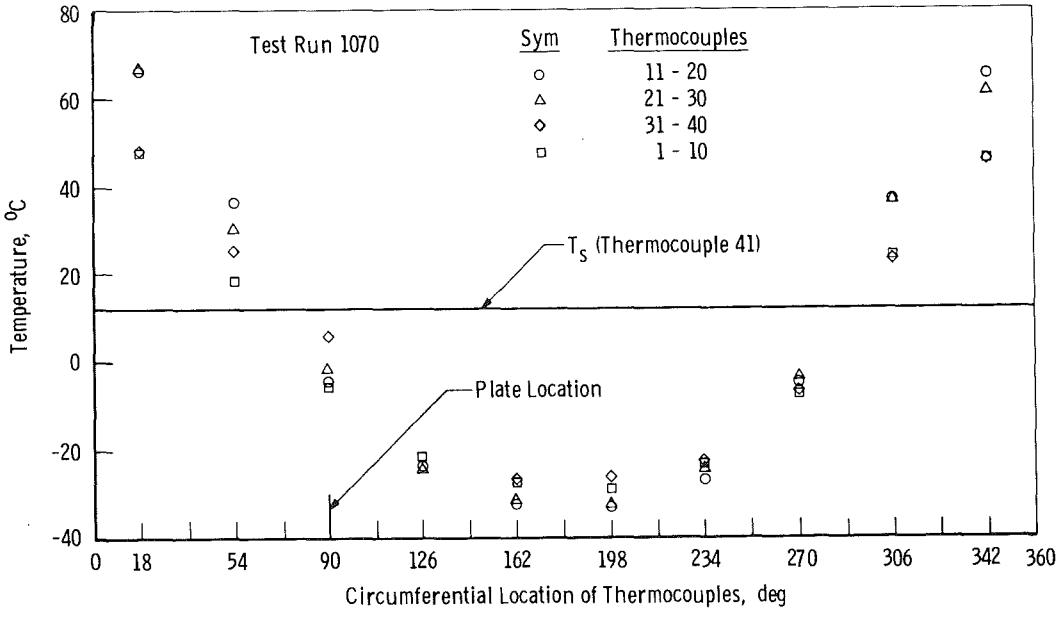

Figure 14. Sphere temperature distribution for unfiltered solar and -190°C plate temperature.

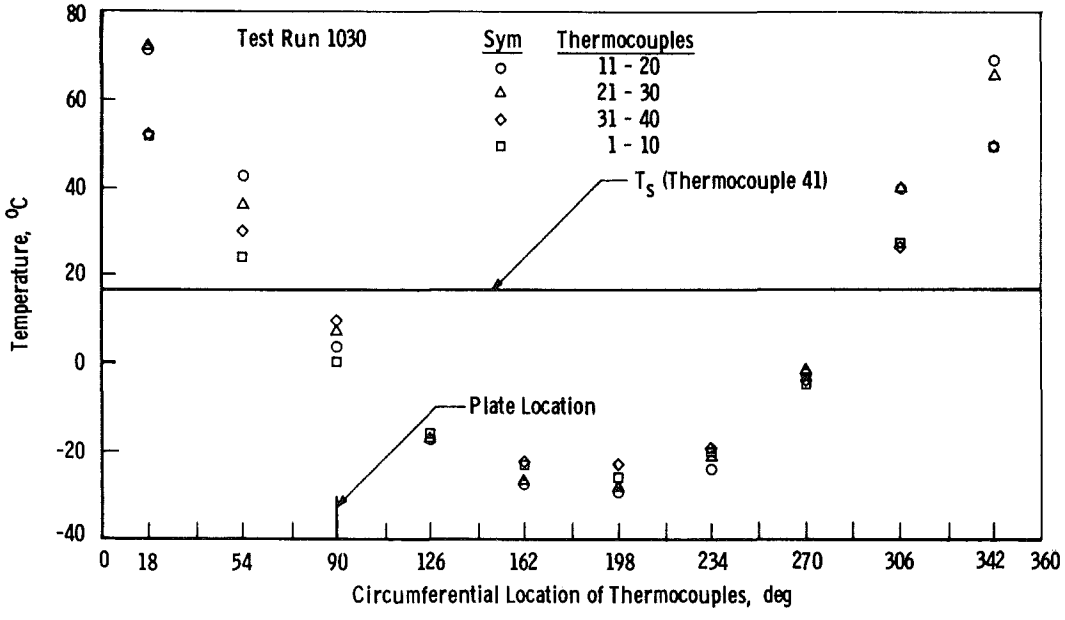

Figure 15. Sphere temperature distribution for filtered solar and 21°C plate temperature.

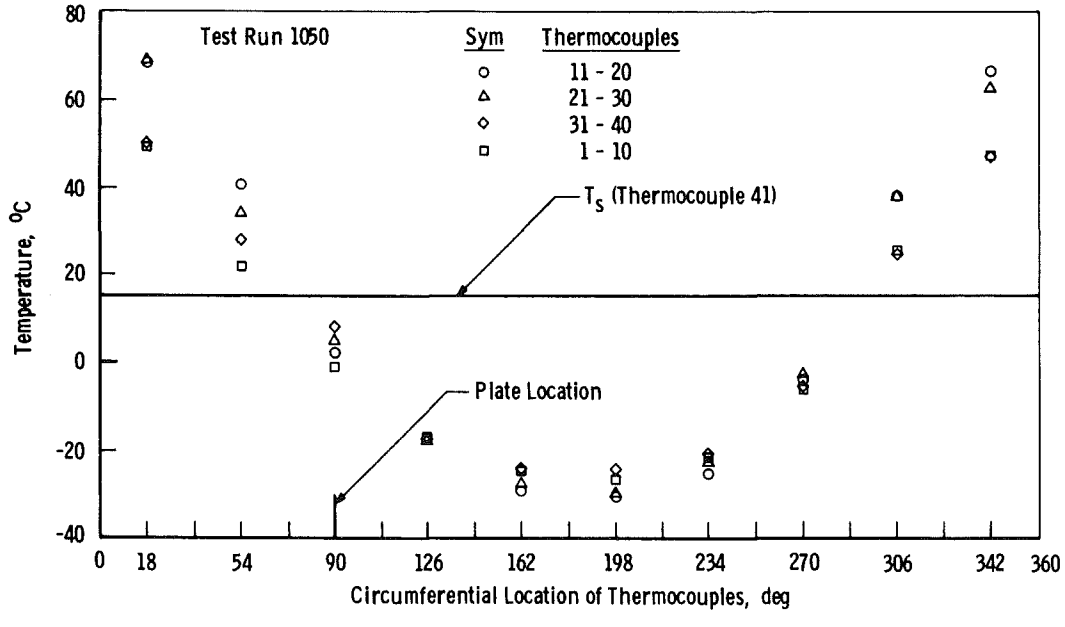

Figure 16. Sphere temperature distribution for unfiltered solar and 21°C plate temperature.

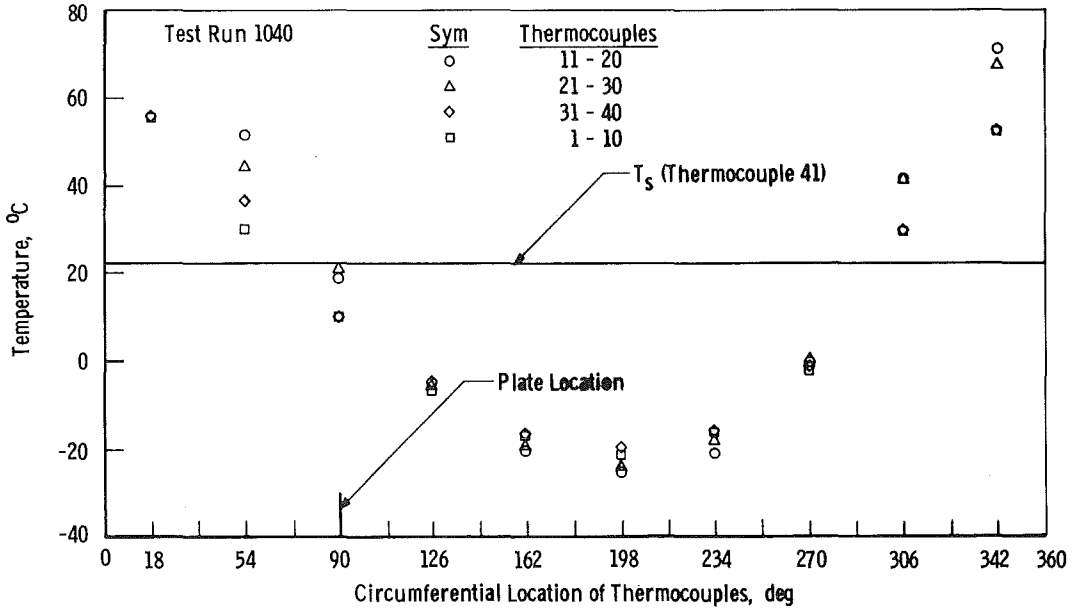

Figure 17. Sphere temperature distribution for filtered solar and 125°C plate temperature.

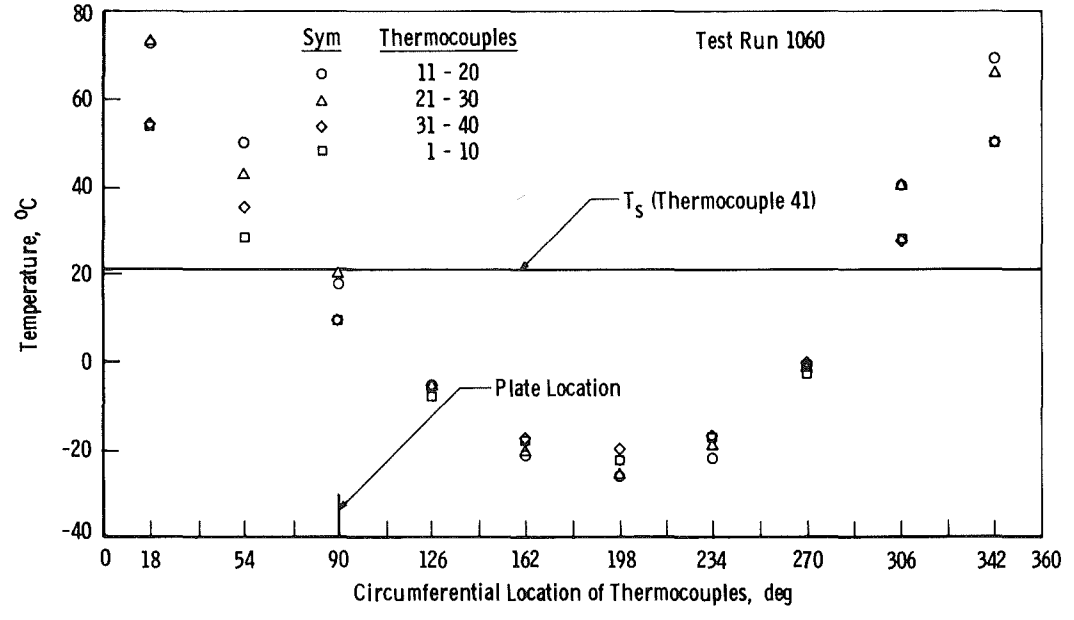

Figure 18. Sphere temperature distribution for unfiltered solar and 125°C plate temperature.

From Figs. 13 and 14, the temperature distribution is seen to be almost perfectly symmetrical; this is because the flat plate is the same temperature as the chamber walls. However, Figs. 15 and 16 show that even at a plate temperature of 21°C the sphere temperature distribution is noticeably affected, the largest temperature difference occurring between the two symmetrical locations nearest and farthest away from the flat plate (i.e., nodes 13 and 18 or nodes 23 and 28). It was felt that with the solar simulator on, the effect of a room temperature hot spot might not be noticeable. The largest difference for the 21°C flat plate for symmetric locations (such as nodes 13 and 18) is only about 6°C. If the sphere were constructed such that thermal conduction in the circumferential direction was significant, then the temperature difference between nodes 13 and 18 would probably be insignificant. This leads one to suspect that a similar size hot spot (30- by 30-cm plate at 21°C) on the chamber wall would have an insignificant effect on a thermal balance test. A room temperature wall hot spot might occur in the form of a viewport, which would be at a greater distance from the model than the presently used flat plate. Thus, its solid angle (or view factor) influence on the test article would be less than that of the flat plate.

From Figs. 17 and 18, the 125°C plate is seen to have a large effect on the temperature distribution as compared to the completely symmetrical temperature distributions of Figs. 13 and 14. The largest temperature difference between two symmetrical sphere elements (i.e., 13 and 18) is about 18°C. For both the filtered and unfiltered cases the integral equilibrium temperature for the -190°C plate was $T_S \approx 14°C$, for the 21°C plate it was $T_S \approx 17°C$, and for the 125°C plate it was $T_S \approx 23°C$.

Figure 19, which was sent from DFVLR, shows that the low temperatures are almost equal to those in Figs. 13 and 14 (i.e., -31°C). However, for the sphere locations which became the hottest, the DFVLR results are about 6°C higher; this higher temperature probably occurred because the DFVLR solar beam is divergent and the flux at the top of the sphere is slightly greater than one solar constant.

Figures 20 and 21 show the typical transient response of the sphere thermocouples when the filtered solar is turned on with the sphere at cold equilibrium. Figure 20 shows the response of the surface thermocouples Nos. 1 through 10, and Fig. 21 shows the response of the inner sphere thermocouple (No. 41). As can be seen, approximately 82 min. are required for the sphere temperatures to reach steady state after

the solar is turned on. Notice that the inner sphere temperature lags the surface temperatures, as would be expected, during the transient phase. The time response with the unfiltered solar is identical.

4.3 PHASE II RESULTS

In Phase II of the test, the solar simulator beam was turned off and an LN_2 platform was installed to cover the ambient temperature collimating mirror. Hence, the sphere was surrounded by black walls cooled to 77°K. With the solar simulator turned off, the effect of a hot spot should have a stronger influence. The temperature distributions shown in Figs. 22, 23, and 24 are for plate temperatures of -190, 21, and 125°C, respectively. For studying the results in this section, please note the sphere orientation in Fig. 12a. Figure 22 shows the sphere temperature distribution under total cold conditions; all of the sphere segments are very close to the integral equilibrium temperature of -156°C.

Figure 23 shows the sphere temperature distribution for a flat plate temperature of 21°C. The maximum temperature difference across the sphere is about 9°C, and the integral equilibrium temperature is about -135°C. The presence of the 21°C flat plate has caused a 21°C temperature difference in the integral equilibrium temperature from the cold conditions. This yields an indication of the effect of an open viewport when one is trying to measure temperature under cold conditions. However, a viewport at a greater distance away from the model would have less of an impact upon the model temperature due to its reduced view factor.

Figures 24 and 25 illustrate a comparison of the results for a 125°C plate temperature for the test conducted at AEDC and DFVLR, respectively. The AEDC results appear to be almost uniformly 6°C higher than the DFVLR results. This would appear to suggest that the DFVLR simulation of a cold background is perhaps somewhat better than the AEDC simulation.

4.4 PHASE III RESULTS

For Phase III, the flat plate was removed from the chamber, the solar was left off, and the mirror inspection platform remained lowered. The sphere sections Nos. 1, 11, 6, 26, and 36 were heated in increments of 0.1, 0.25, 0.5, 0.75, and 1.0 w in the sequence described in Table 2. For each test run, the equilibrium temperatures of all 40 surface thermocouples were plotted versus the thermocouple number, with the integral equilibrium temperature plotted as a straight line across the figure.

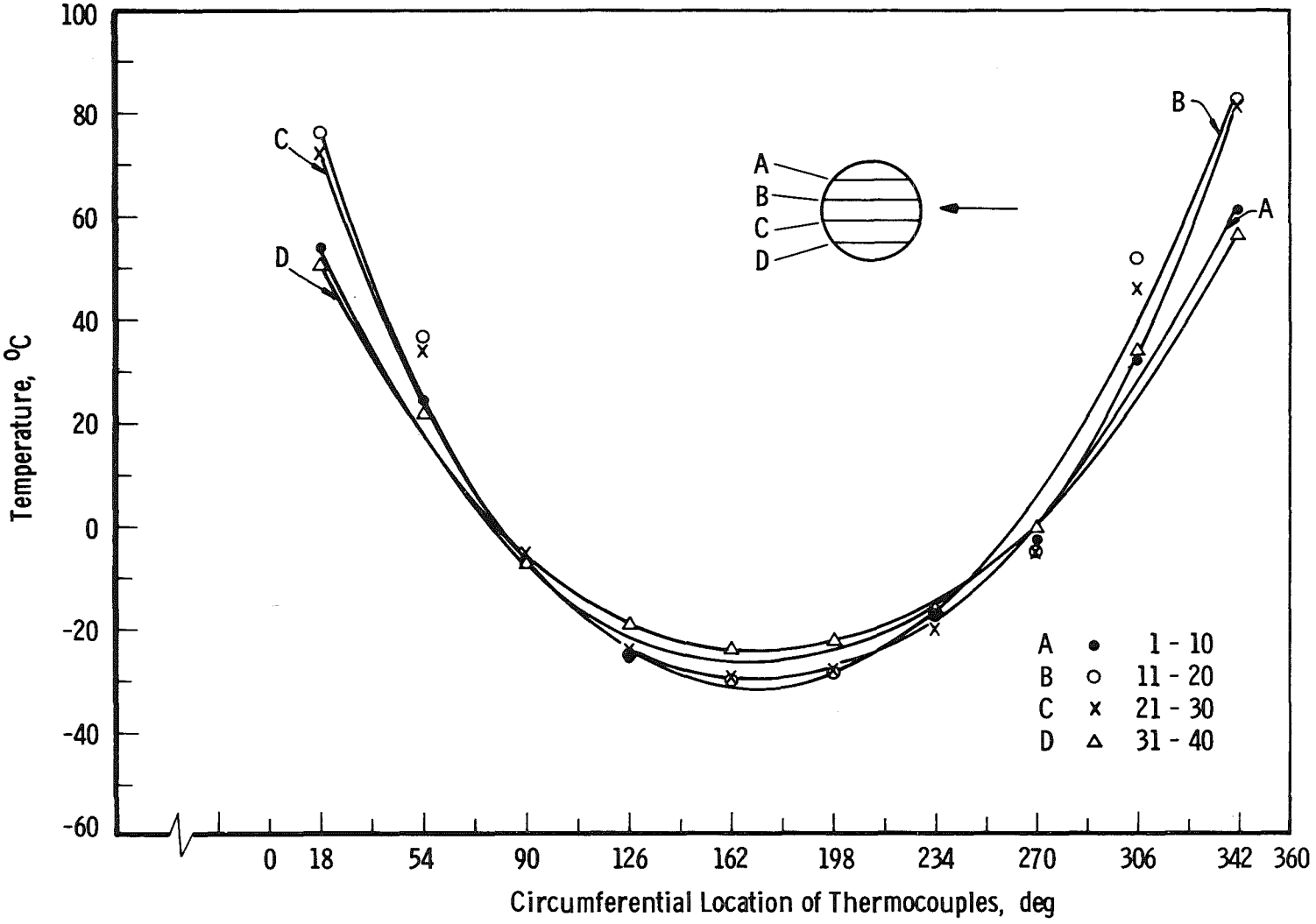

Figure 19. Sphere temperature distribution via DFVLR with solar simulator and no hot spot.

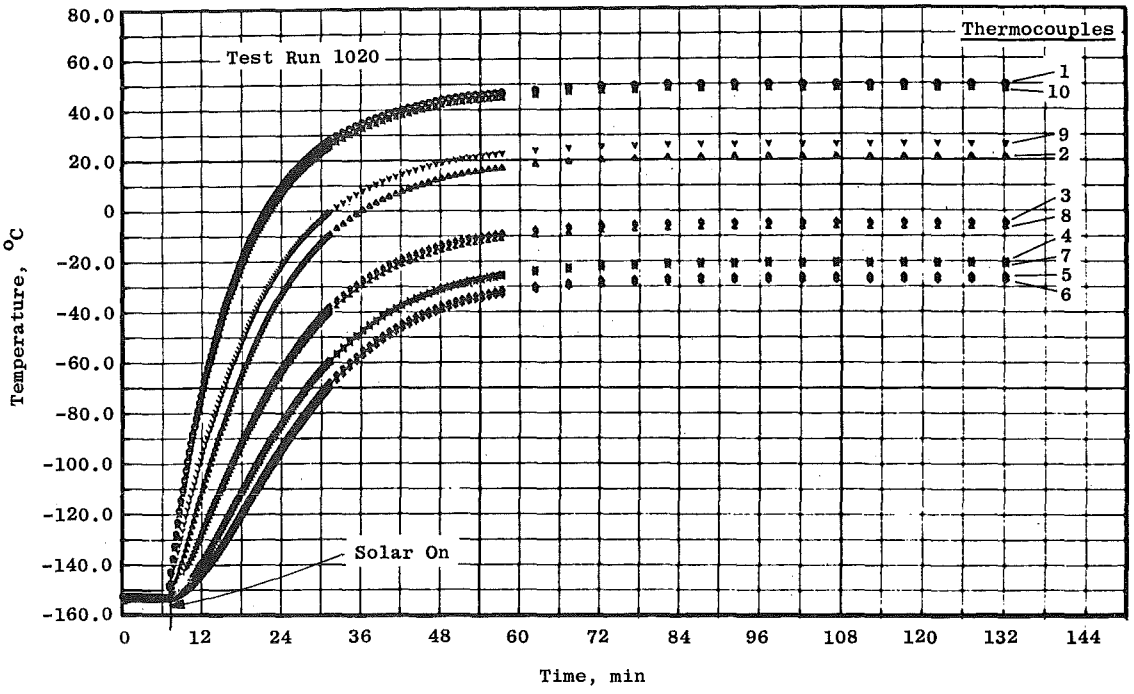

Figure 20. Transient response of surface thermocouples 1 through 10 with filtered solar.

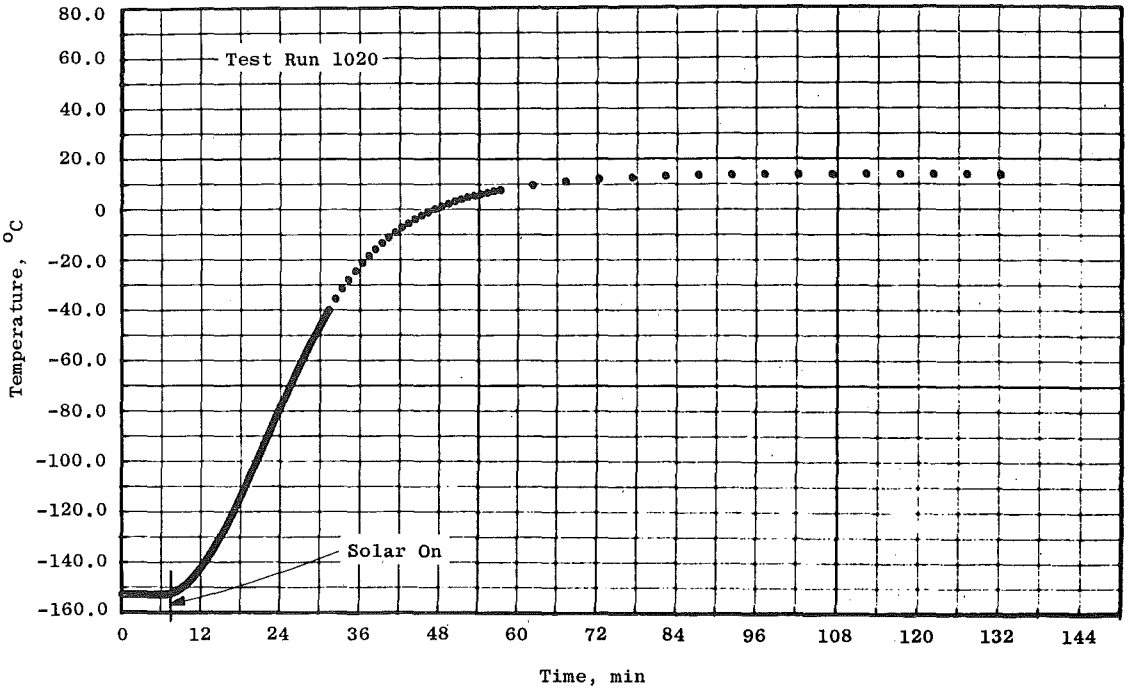

Figure 21. Transient response of the inner sphere thermocouple (No. 41) with filtered solar.

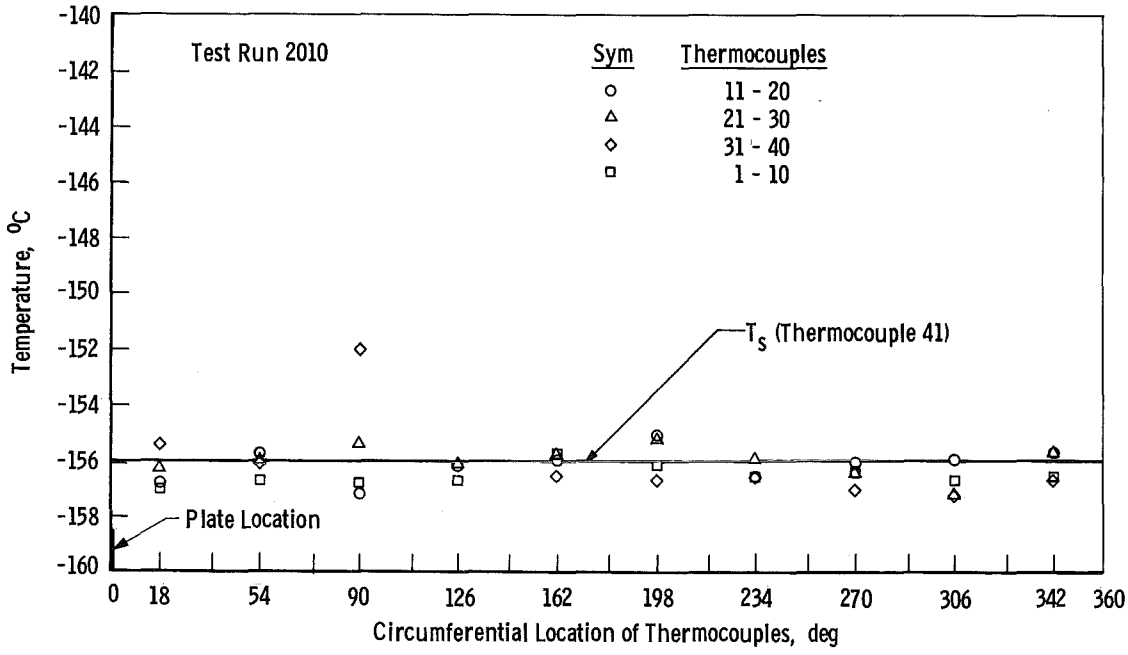

Figure 22. Sphere temperature distribution for cold conditions.

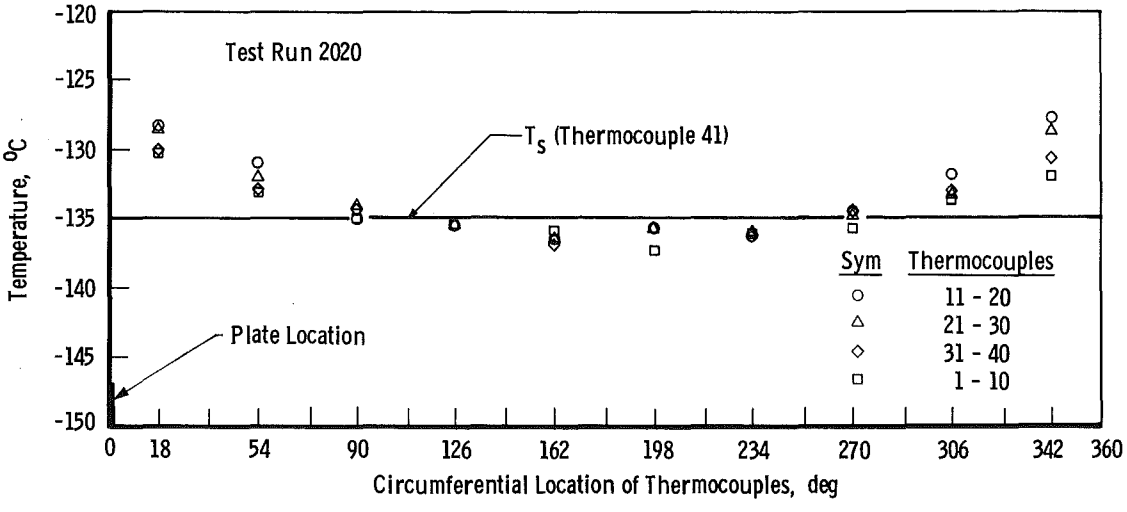

Figure 23. Sphere temperature distribution for 21°C plate temperature without solar simulation.

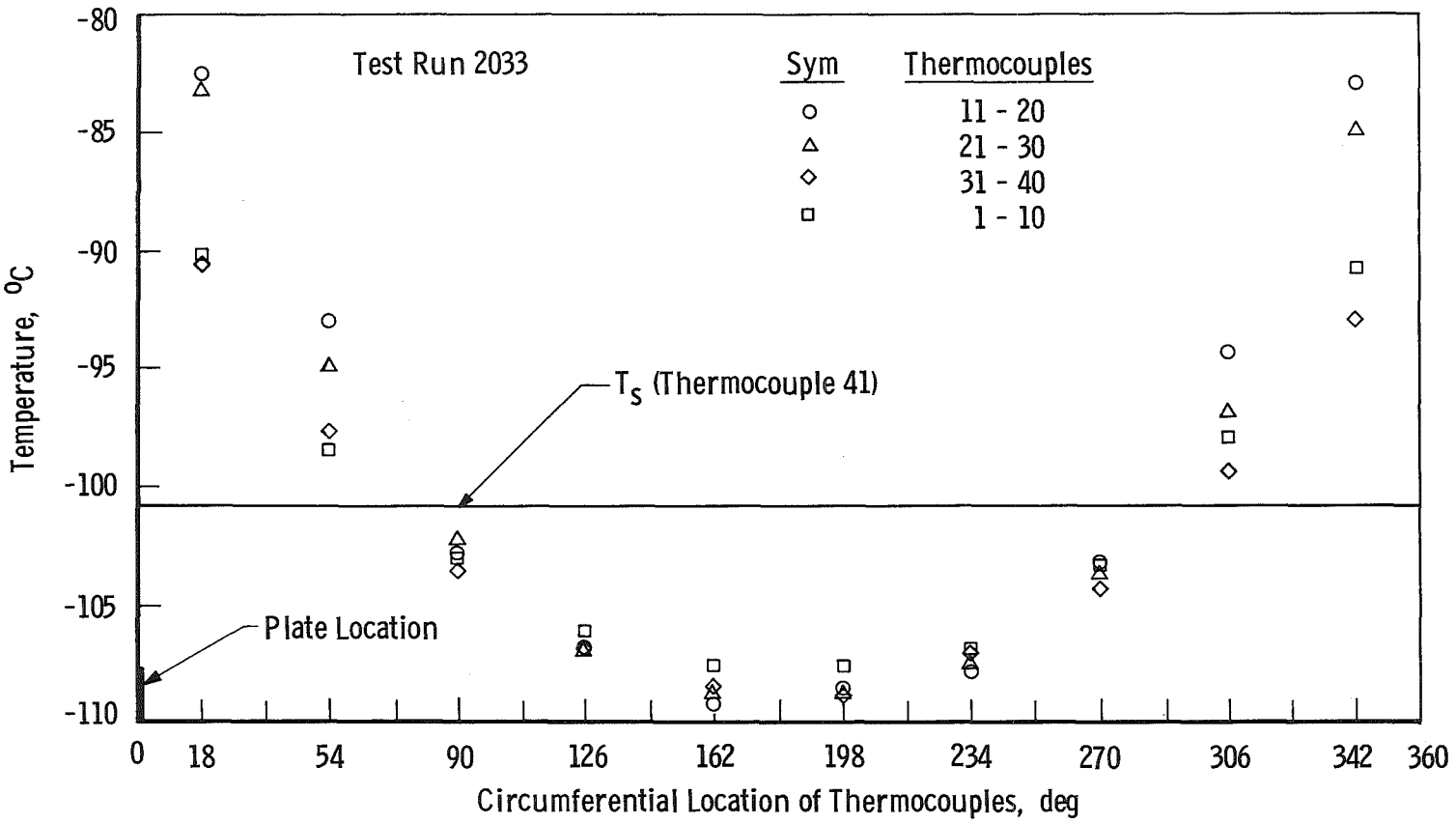

Figure 24. Sphere temperature distribution for 125°C plate temperature without solar simulation.

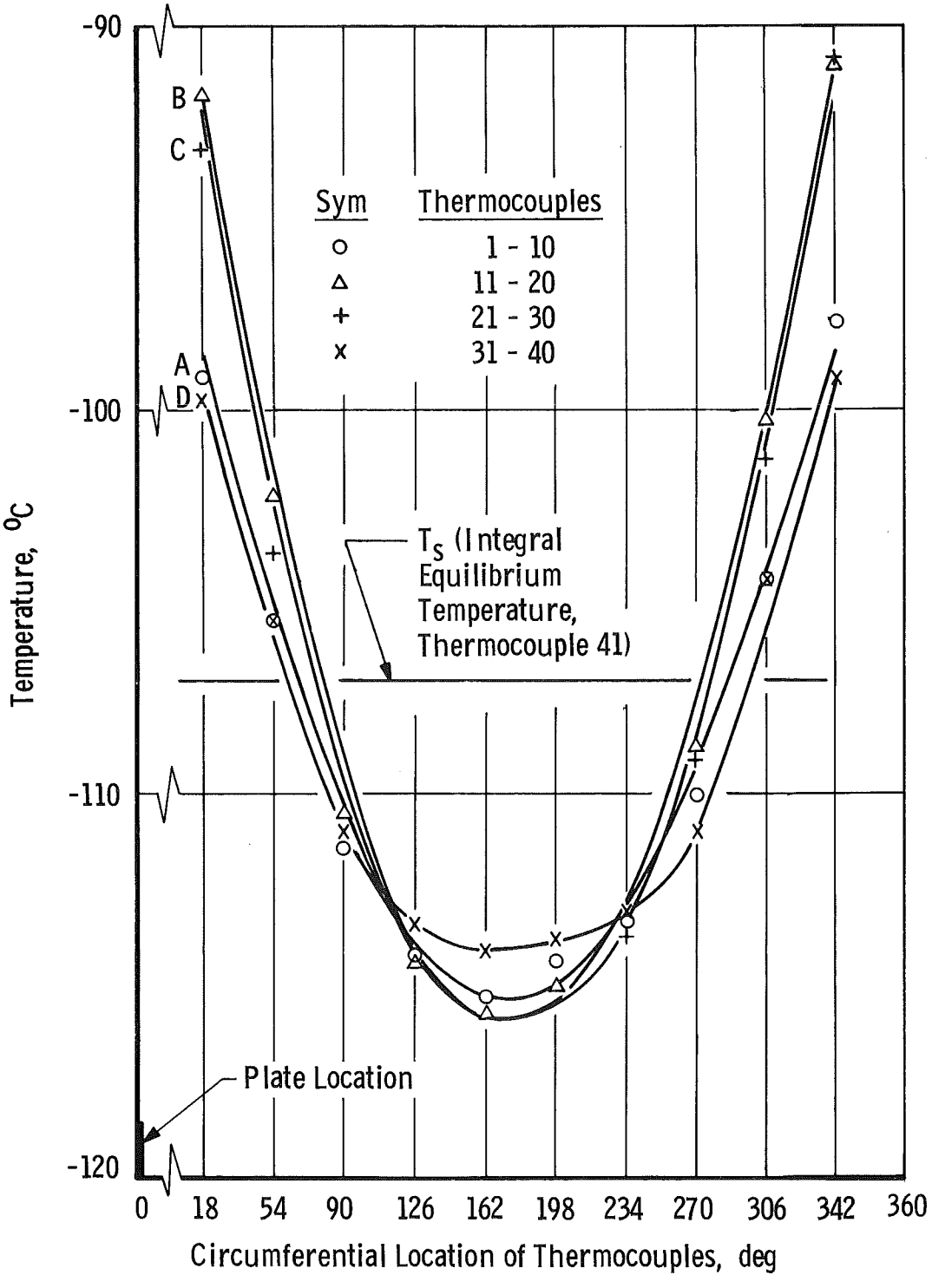

Figure 25. DFVLR results for sphere temperature distribution for 125°C plate temperatures without solar simulation (Ref. 6).

Figure 26 shows the temperature distribution over the sphere surface under cold equilibrium conditions, with a ±1°C variation evident. It is felt that a significant amount of this variation is due to individual thermocouple or data system errors and not to localized "hot spots" in the chamber cryosurfaces. Figures 27 through 31 show the temperature distribution over the sphere surface with surface segment 1 heated with 0.1, 0.25, 0.5, 0.75, and 1.0 w, respectively. Figure 32 shows the corresponding temperature distributions as determined "theoretically" by DFVLR (Ref. 6). Absolute comparison between the theoretical and measured results is difficult because of the initial measured temperature distribution before heat was applied. In addition, the theoretical integral equilibrium is -178°C compared to the measured value of -153.8°C. However, the relative temperature changes can be used for comparison. Table 5 shows the relative theoretical and measured temperature changes from the respective equilibrium conditions for the thermocouples on the heated segments.

As seen in the table, the change in temperature is approximately 30 to 50 percent less for the measured results than for the theoretical analysis. One explanation is that the sphere at the higher measured temperatures will radiate more energy per surface area than will the analytical model at the lower temperatures, and the result will be less temperature change from the unheated values. However, it is felt that this has a relatively minor effect and that the biggest experimental problem is radiation heat loss directly from the strip heaters to other sphere segments. Thus, not all of the wattage which is applied to the heaters is conducted directly to the segment on which the heaters are mounted. Otherwise, the measured values in Table 1 show a variation from run to run which is very consistent with the corresponding variation for the theoretical values.

Figures 33 through 37 show the temperature distribution over the sphere surface with segment 11 heated with 0.1, 0.25, 0.5, 0.75, and 1.0 w, respectively. Figure 38 shows the corresponding temperature distribution as determined theoretically by DFVLR. Figures 39 through 42 show the results with segment 11 heated to 1.0 w and segments 6, 16, 26, and 36 heated to 0.5 w, respectively. The corresponding theoretical results are shown in Figs. 43 through 46, respectively.

The cold equilibrium condition shown in Fig. 26 was measured before the test runs in Figs. 27 through 31 and in Figs. 39 and 40. Figure 47 shows an additional cold equilibrium condition that was measured before the test runs in Figs. 33 through 37, 41, and 42.

The remaining thermocouples not listed in Table 5 showed the same general distribution trends (with the limits of the individual thermocouple errors) as the theoretical data. However, in all of the tests, the measured integral equilibrium temperature did not change as much (percentage-wise, relative to the change of the surface thermocouples) as did the theoretical integral equilibrium temperature.

The results of Phase III give some idea of the sensitivity of the sphere to incident energy from chamber hot spots. When the analytical results were analyzed, it was concluded that "the sphere can only be applied conditionally for investigation of heat losses which are smaller than 0.25 w at a segment" (Ref. 6, p. 19). This conclusion is reinforced by the test results, which show less than a 1°C temperature difference between heated and unheated segments at wattage levels of 0.25 w or lower. This is within the range of the thermocouple and data system errors.

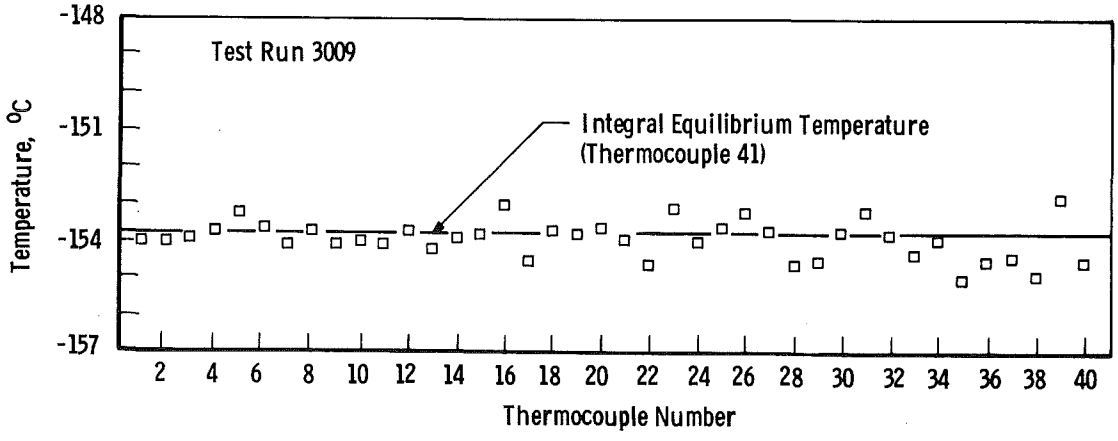

Figure 26. Sphere temperature distribution for cold equilibrium condition.

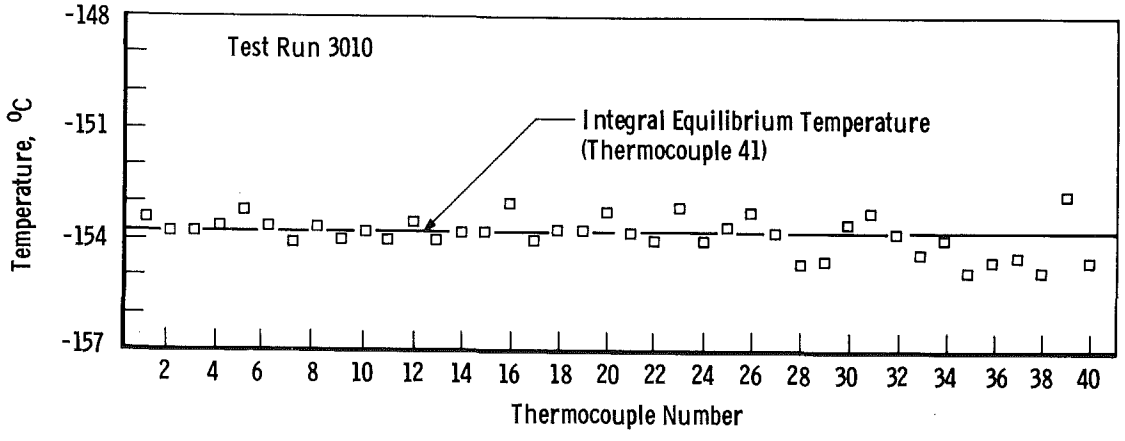

Figure 27. Sphere temperature distribution, segment 1 heated with 0.1 w.

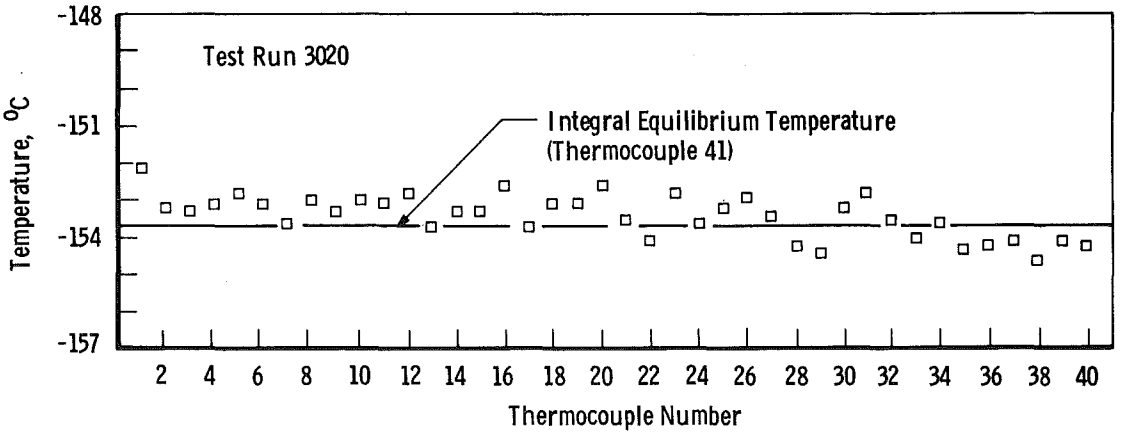

Figure 28. Sphere temperature distribution, segment 1 heated with 0.25 w.

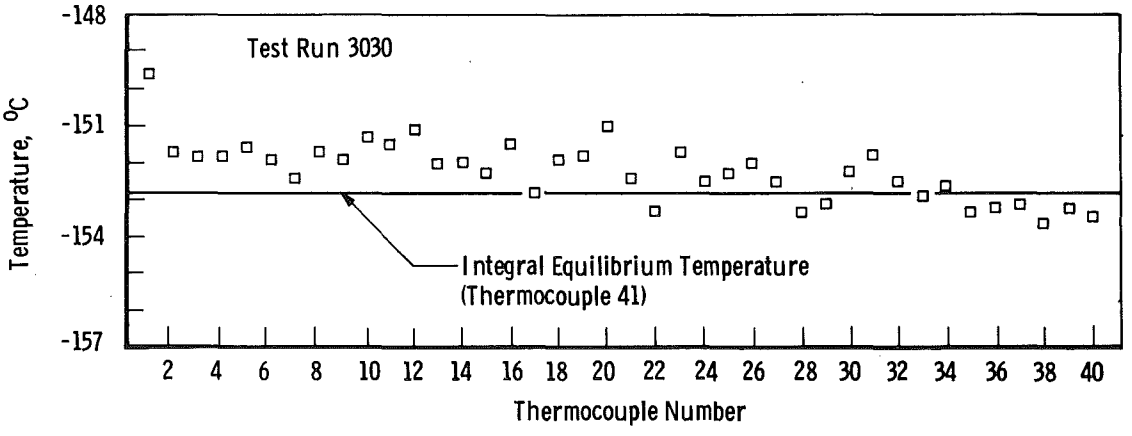

Figure 29. Sphere temperature distribution, segment 1 heated with 0.5 w.

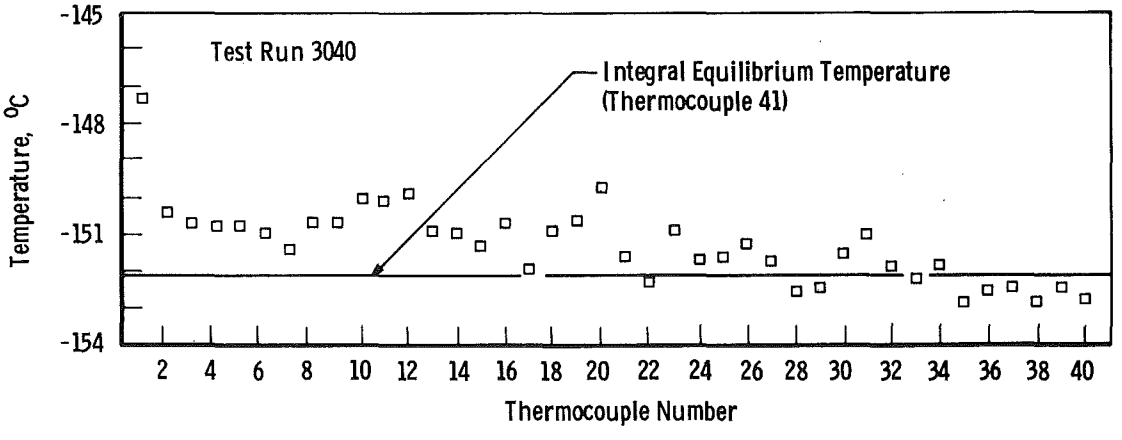

Figure 30. Sphere temperature distribution, segment 1 heated with 0.75 w.

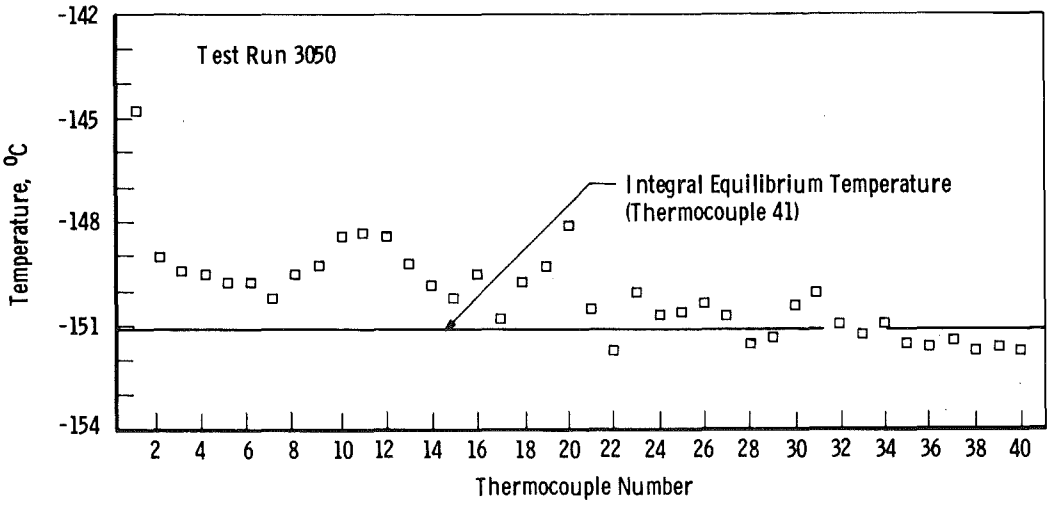

Figure 31. Sphere temperature distribution, segment 1 heated with 1.0 w.

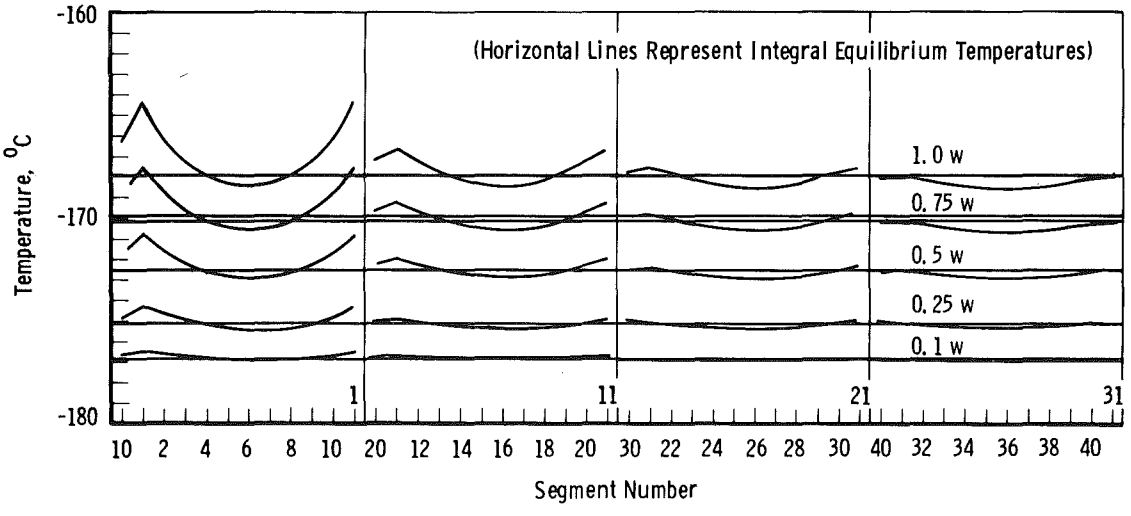

Figure 32. Analytical sphere temperature distribution, segment 1 heated (Ref. 6).

Table 5. Comparison of Theoretical and Measured Results for Phase III

Segments	Watts	Temperature Change from Equilibrium		
		Thermocouple Number	Theoretical, °C	Measured, °C
1	0.1	1	+ 1.4	+ 0.6
1	0.25	1	+ 3.8	+ 1.9
1	0.5	1	+ 7.1	+ 4.4
1	0.75	1	+10.4	+ 6.7
1	1.0	1	+13.8	+ 9.2
11	0.1	11	+ 1.3	+ 0.7
11	0.25	11	+ 3.5	+ 1.8
11	0.5	11	+ 6.8	+ 4.6
11	0.75	11	+ 9.9	+ 6.9
11	1.0	11	+14.0	+ 9.0
11	1.0	11	+16.7	+10.6
6	0.5	6	+15.4	+ 8.8
11	1.0	11	+16.7	+10.8
16	0.5	16	+14.9	+ 8.4
11	1.0	11	+16.7	+11.5
26	0.5	26	+14.9	+ 8.9
11	1.0	11	+16.7	+11.5
36	0.5	36	+15.4	+ 9.8

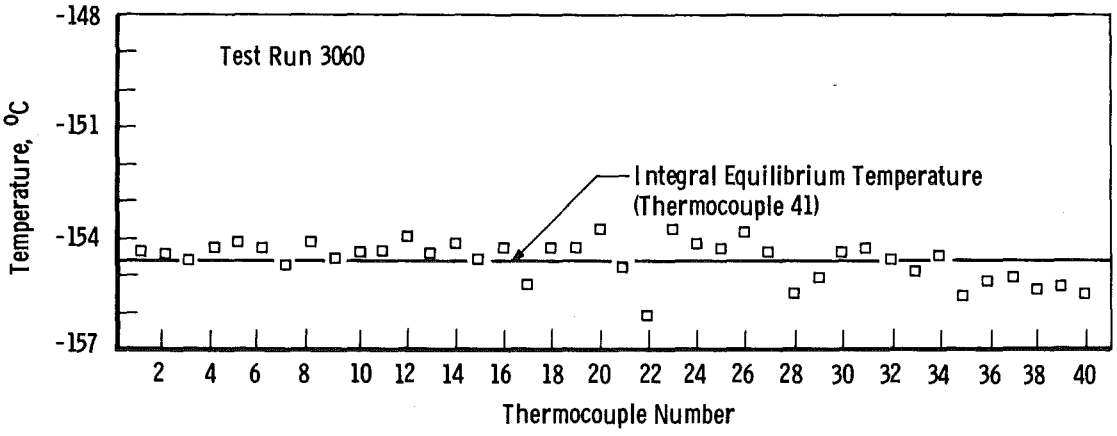

Figure 33. Sphere temperature distribution, segment 11 heated with 0.1 w.

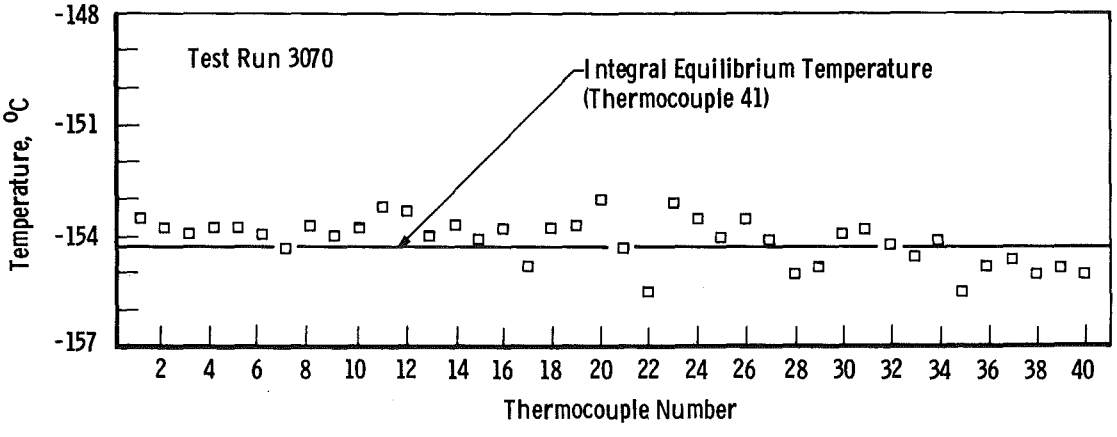

Figure 34. Sphere temperature distribution, segment 11 heated with 0.25 w.

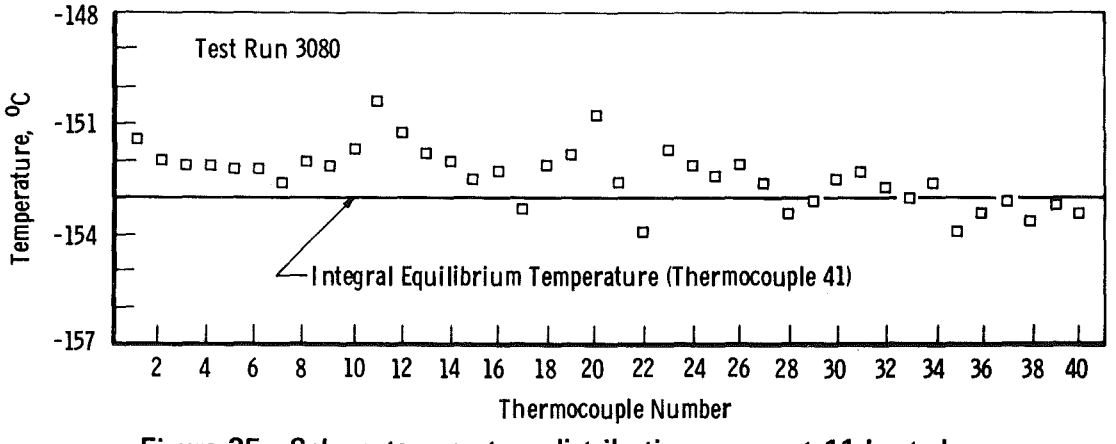

Figure 35. Sphere temperature distribution, segment 11 heated with 0.5 w.

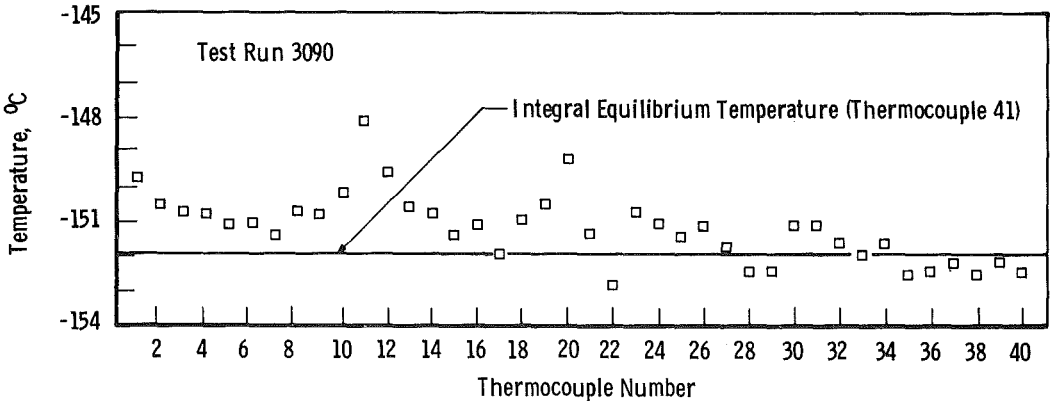

Figure 36. Sphere temperature distribution, segment 11 heated with 0.75 w.

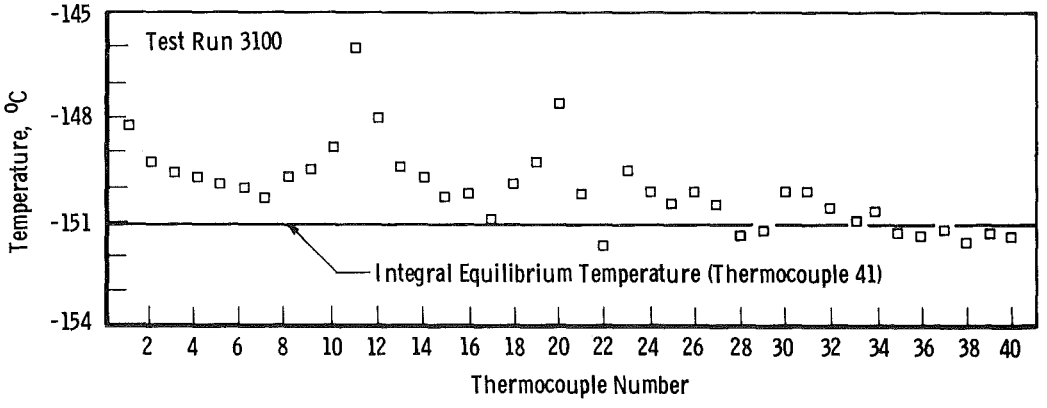

Figure 37. Sphere temperature distribution, segment 11 heated with 1.0 w.

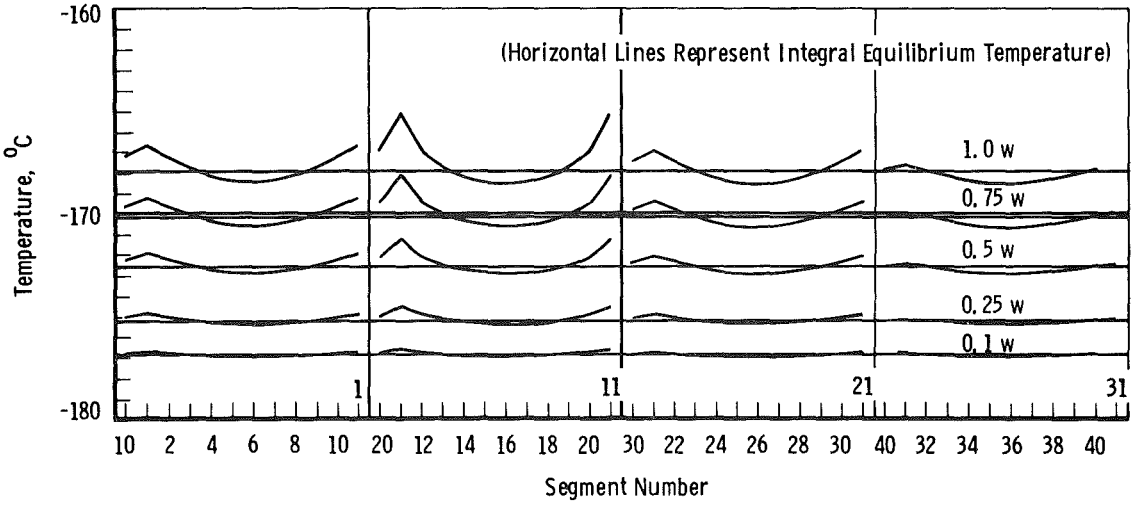

Figure 38. Analytical sphere temperature distribution, segment 11 heated (Ref. 6).

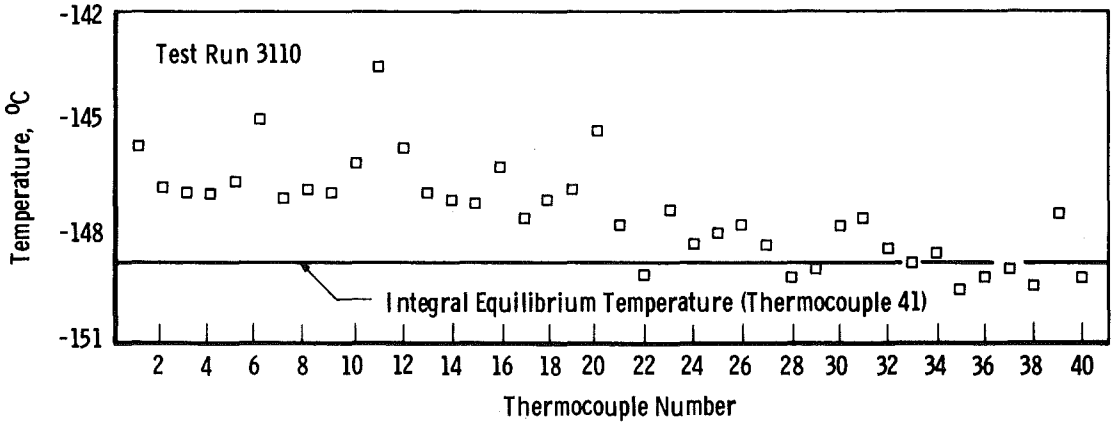

Figure 39. Sphere temperature distribution, segment 11 heated with 1.0 w and segment 6 heated with 0.5 w.

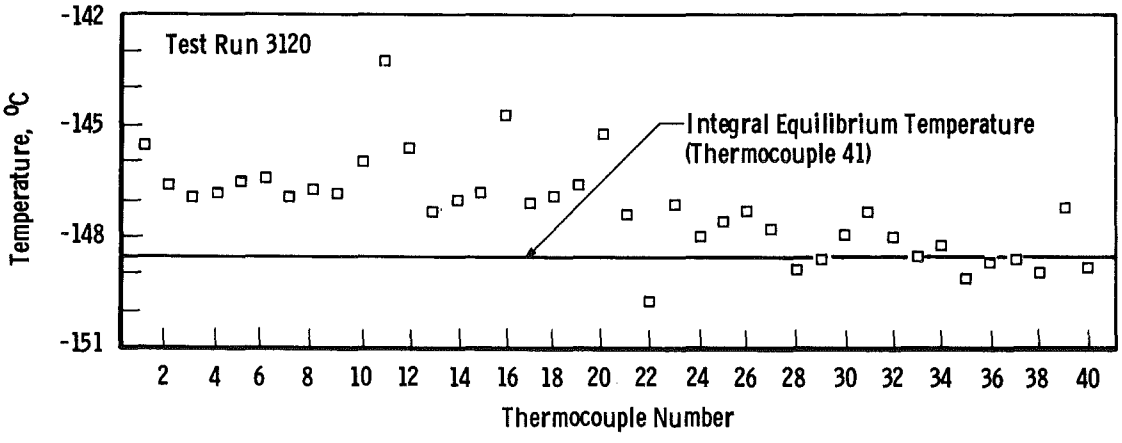

Figure 40. Sphere temperature distribution, segment 11 heated with 1.0 w and segment 16 heated with 0.5 w.

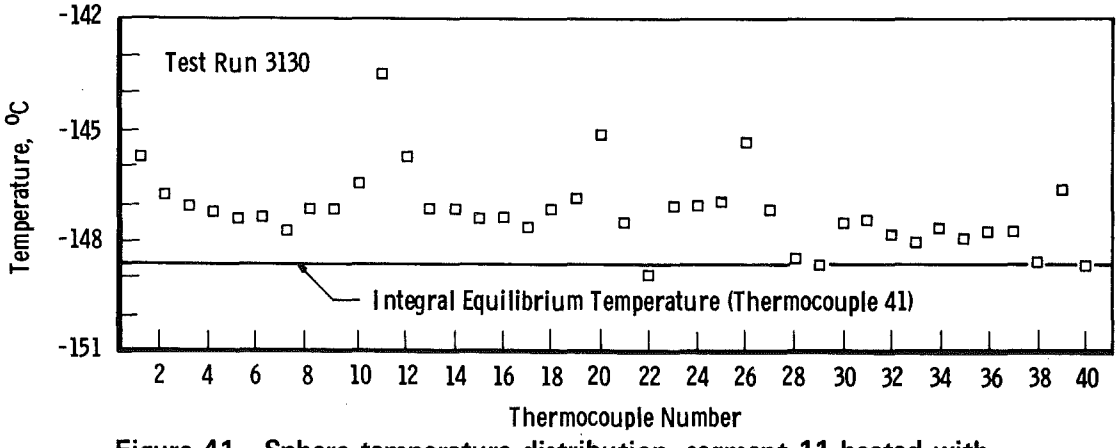

Figure 41. Sphere temperature distribution, segment 11 heated with 1.0 w and segment 26 heated with 0.5 w.

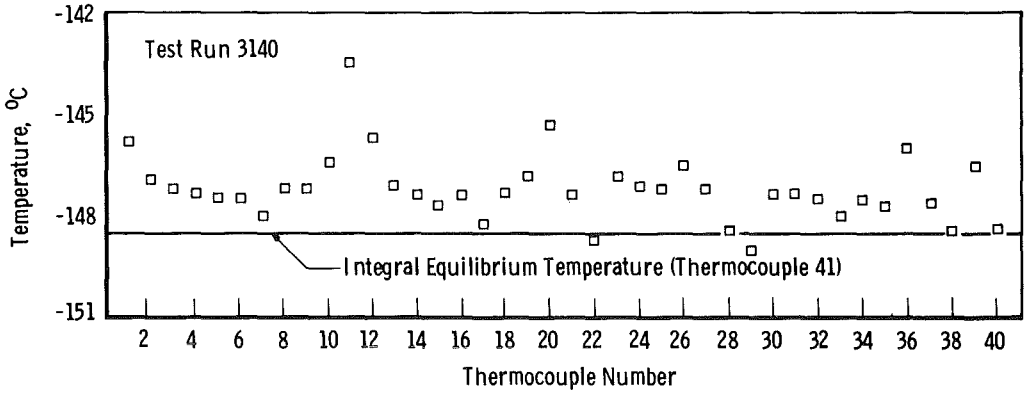

Figure 42. Sphere temperature distribution, segment 11 heated with 1.0 w and segment 36 heated with 0.5 w.

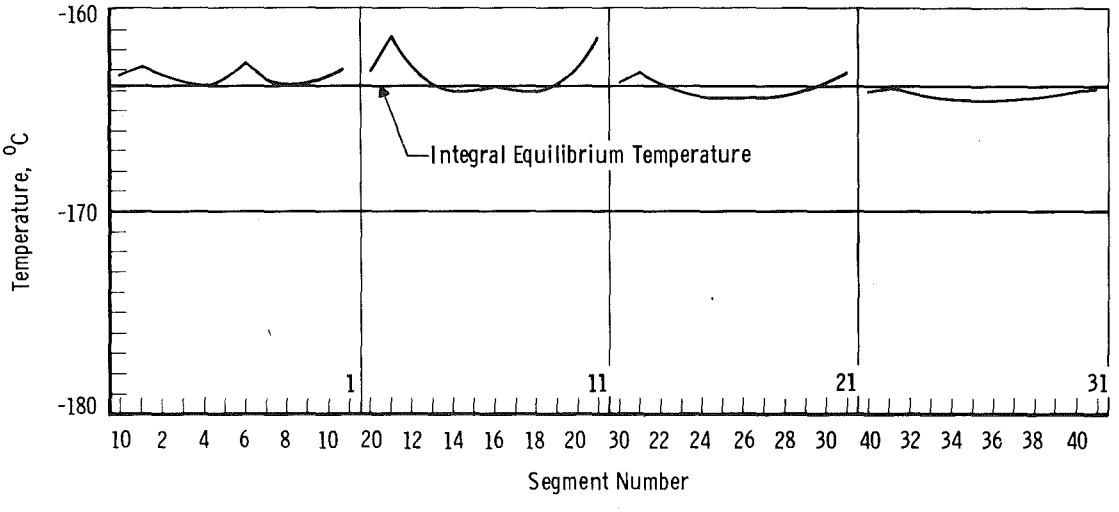

Figure 43. Analytical sphere temperature distribution, segment 11 heated with 1.0 w and segment 6 heated with 0.5 w (Ref. 6).

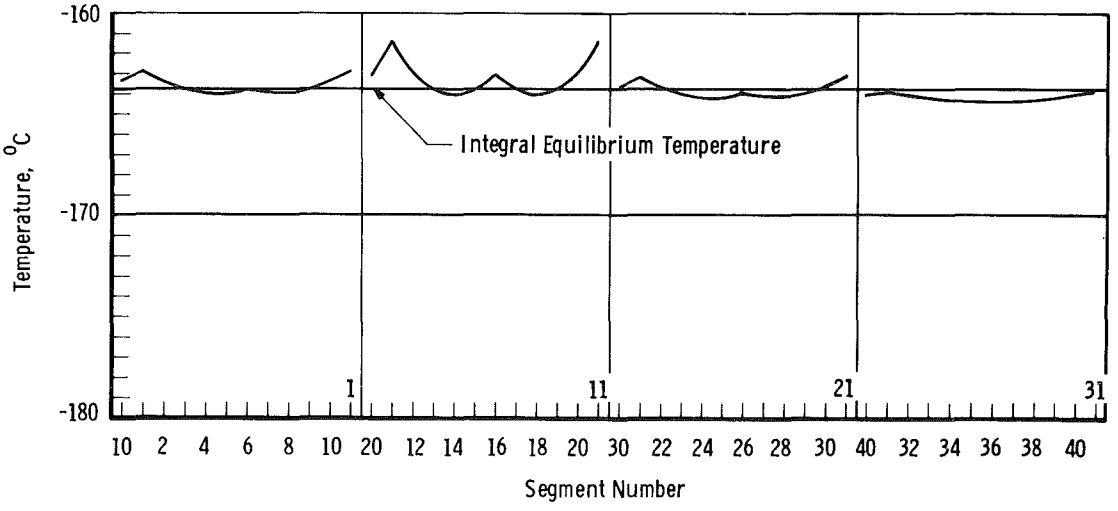

Figure 44. Analytical sphere temperature distribution, segment 11 heated with 1.0 w and segment 16 heated with 0.5 w (Ref. 6).

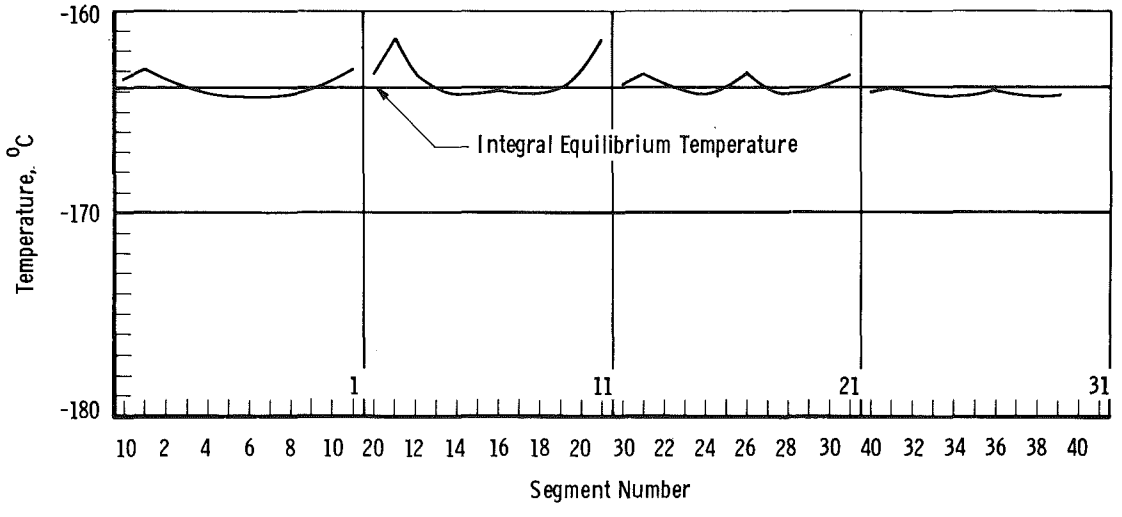

Figure 45. Analytical sphere temperature distribution, segment 11 heated with 1.0 w and segment 26 heated with 0.5 w (Ref. 6).

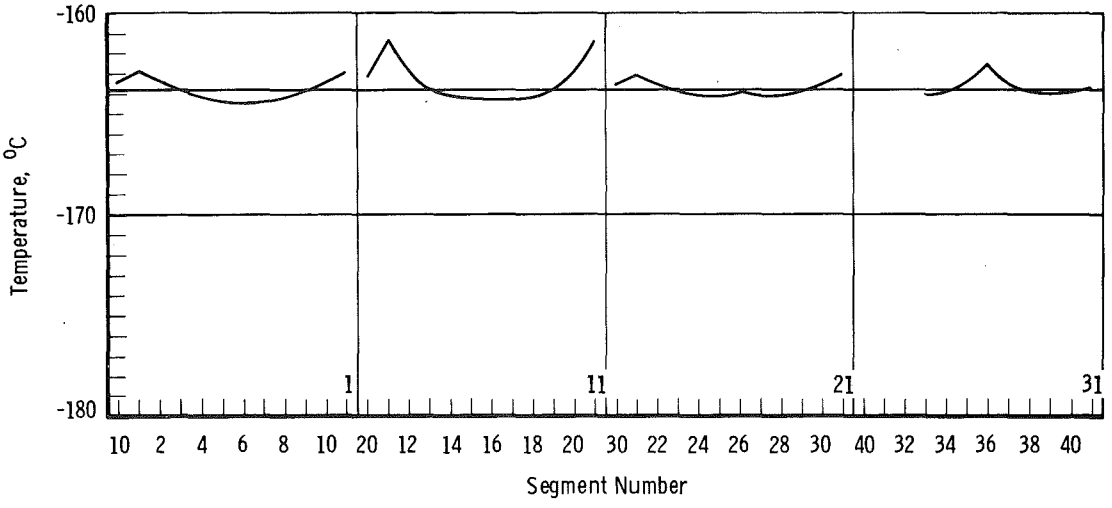

Figure 46. Analytical sphere temperature distribution, segment 11 heated with 1.0 w and segment 36 heated with 0.5 w (Ref. 6).

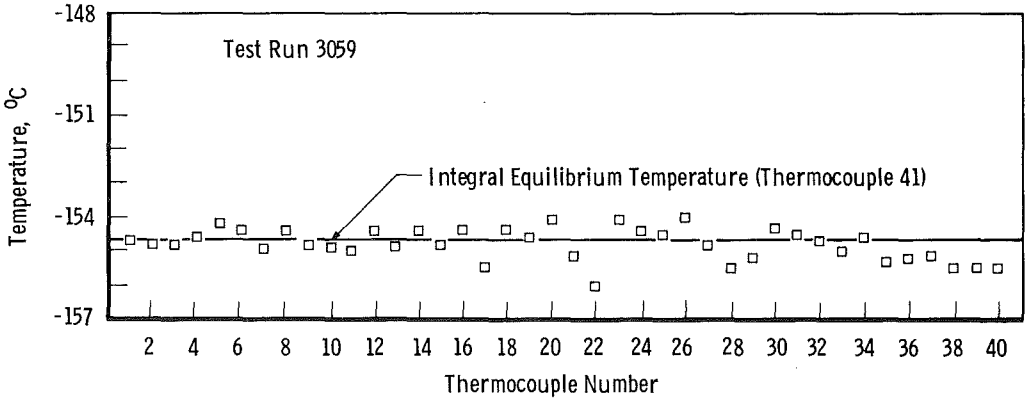

Figure 47. Sphere temperature distribution under cold equilibrium conditions.

4.5 PHASE IV RESULTS

The results of Phase IV are shown in Figs. 48 through 58 and in Table 6. In Fig. 48 the calibration blackbody is shown in the lower left-hand part of the picture. The sphere is not seen because its temperature is about -100°C. Figure 48 is important because it illustrates that there is no reflection problem (sphere emissivity $\approx$ 0.95) in Chamber 12V in the 2- to 5-μm wavelength range due to the solar simulator. If reflection was a problem, then the sphere would be seen because of its reflecting of 2 to 5 μm radiation energy. In Fig. 48 the shutter for the solar simulator has been open for about 2 min, but the temperature of the sphere is so low that its emitted energy cannot be detected by the IR scanning camera.

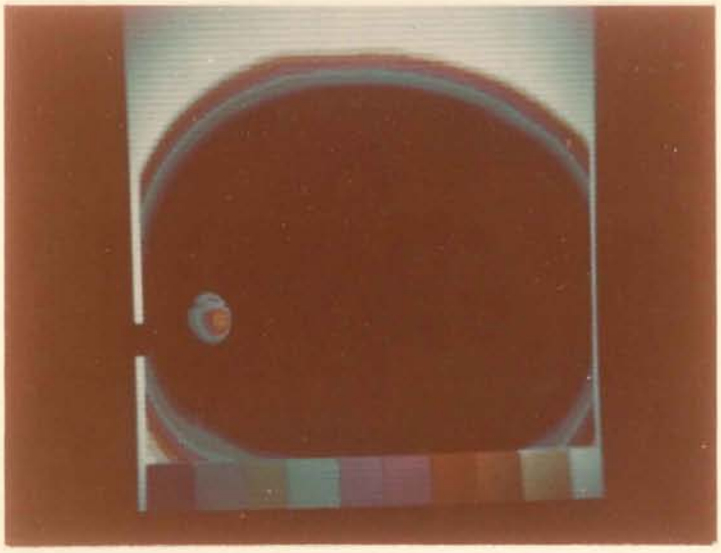

Figure 48. IR camera picture of 27°C blackbody with cold sphere (T ≈ -100°C) and solar simulation (camera setting: sensitivity = 10).

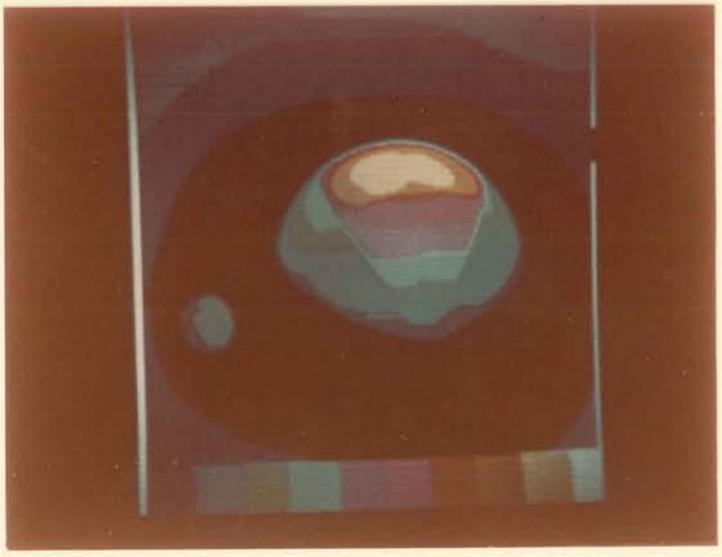

Figure 49. IR camera picture of 35°C blackbody with sphere heated by solar simulator (camera setting: sensitivity = 100).

Blank page

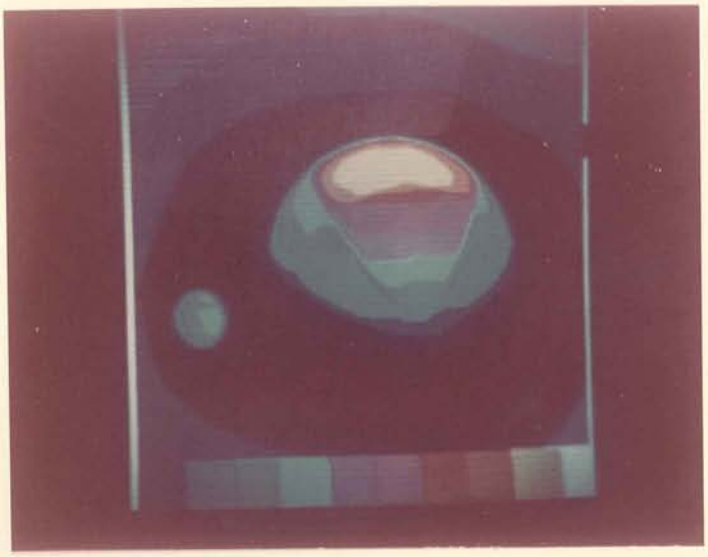

Figure 50. IR camera picture of 49°C blackbody with sphere heated by solar simulator (camera setting: sensitivity = 100).

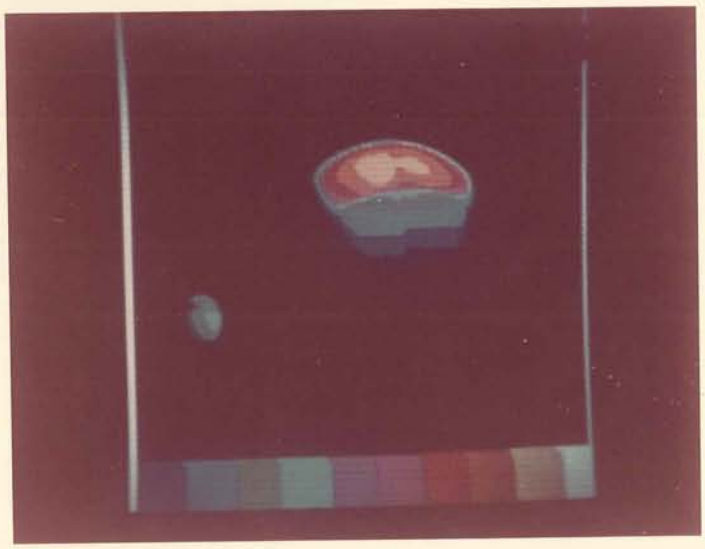

Figure 51. IR camera picture of 63°C blackbody with sphere heated by solar simulator (camera setting: sensitivity = 50).

Blank page

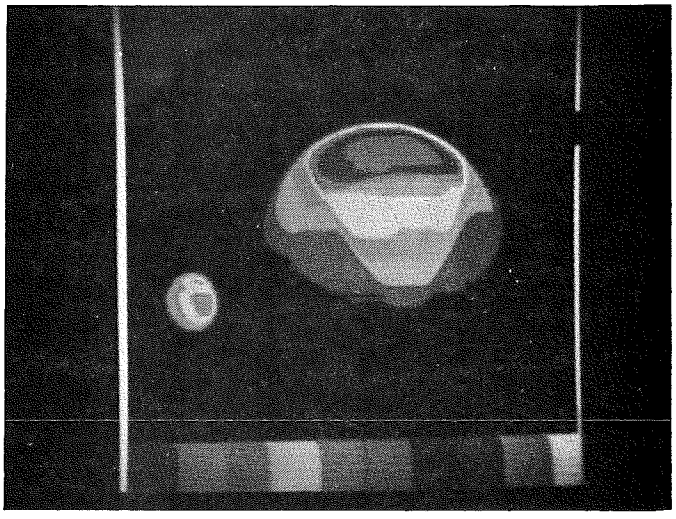

Figure 52. IR camera picture of 65°C blackbody with sphere heated by solar simulator (camera setting: sensitivity = 100).

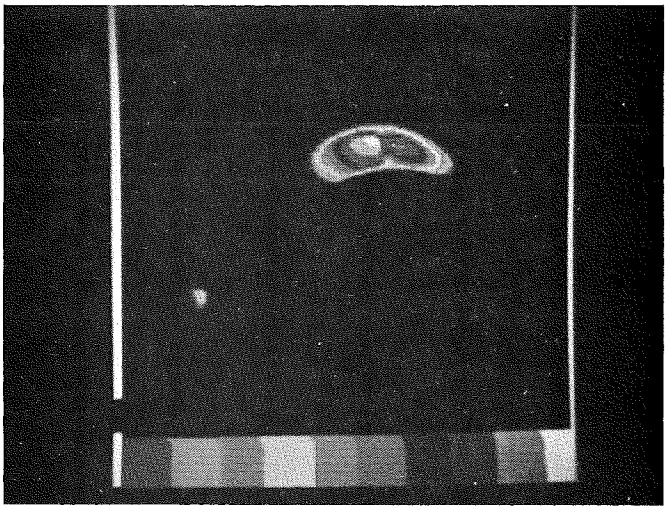

Figure 53. IR camera picture of 70°C blackbody with sphere heated by solar simulator (camera setting: sensitivity = 20).

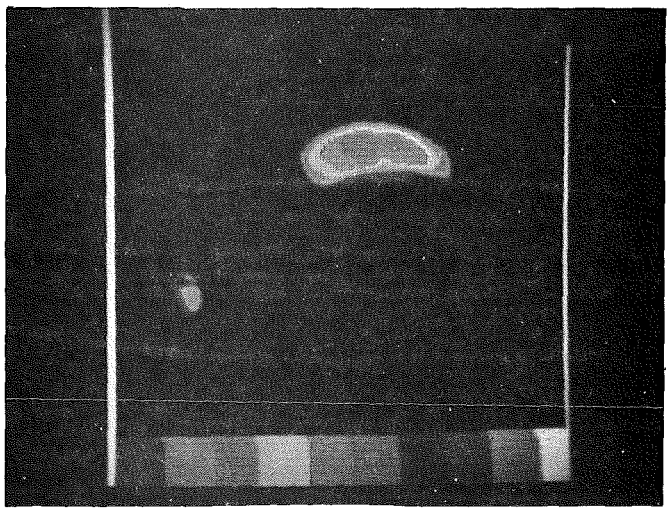

Figure 54. IR camera picture of 70°C blackbody with sphere heated by solar simulator (camera setting: sensitivity = 50).

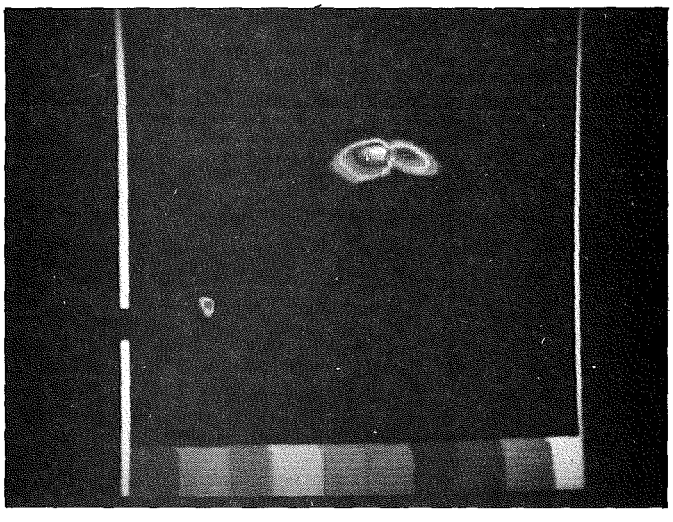

Figure 55. IR camera picture of 75°C blackbody with sphere heated by solar simulator (camera setting: sensitivity = 10).

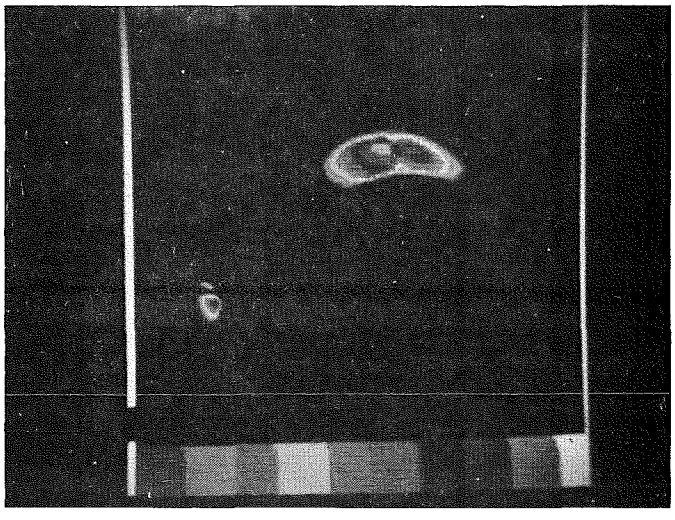

Figure 56. IR camera picture of 75°C blackbody with sphere heated by solar simulator (camera setting: sensitivity = 20).

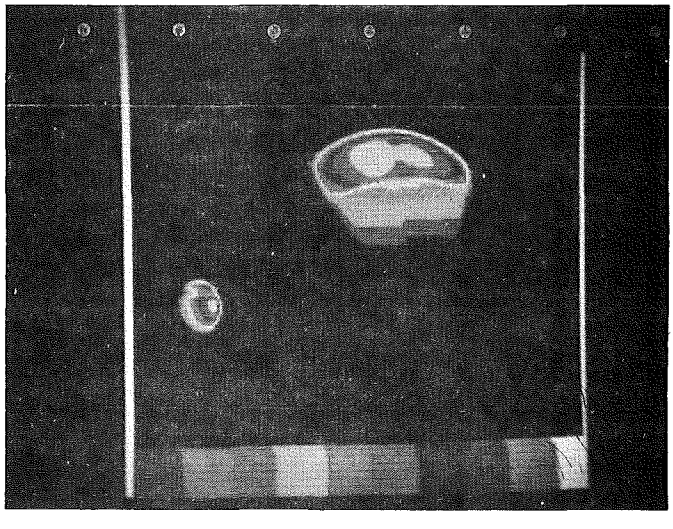

Figure 57. IR camera picture of 75°C blackbody with sphere heated by solar simulator (camera setting: sensitivity = 50).

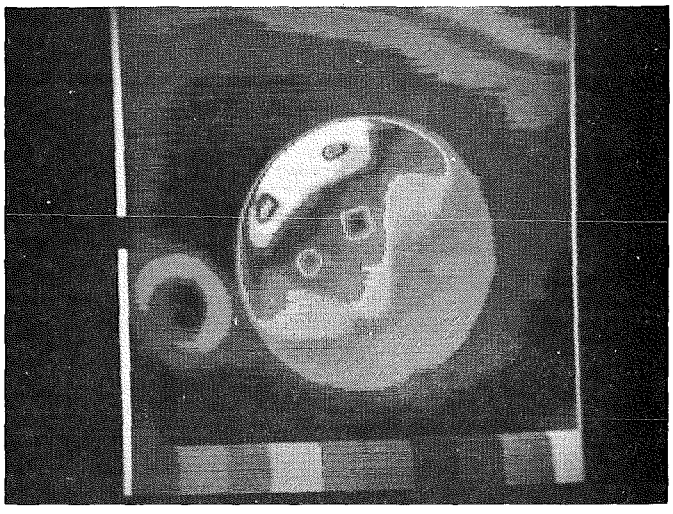

Figure 58. IR camera picture showing the location of thermocouples Nos. 1, 10, 11, and 20 (see also Fig. 12b).

Table 6. Comparison of IR Camera Results with Thermocouple Data

Fig. No.	Camera Sensitivity	Blackbody Temp., °C	Camera-Indicated Temp., °C Sphere Segment Number				Thermocouple-Indicated Temp., °C Sphere Segment Number			
			11	1	20	10	11	1	20	10
49	100	35	72±2	56±3	43±4	32±4	71.4	54.8	42.1	30.3
50	100	49	71±2	55±3	43±4	33±4	72.0	55.6	42.9	31.1
51	50	63	71±1	NA*	NA	NA	71.2	54.8	42.2	30.6
52	100	65	71±2	50±3	43±4	NA	71.4	55.0	42.3	30.7
53	20	70	71±1	NA	NA	NA	71.8	55.3	42.6	30.9
54	50	70	71±1	NA	NA	NA	71.8	55.4	42.7	31.0
55	10	75	71±1	NA	NA	NA	72.3	55.7	43.1	31.4
56	20	75	71±1	NA	NA	NA	72.0	55.5	42.8	31.2
57	50	75	71±1	NA	NA	NA	72.0	55.5	42.8	31.2

*Outside of camera temperature span setting.

In Figs. 49 through 57 a variety of IR camera sensitivity settings and blackbody reference temperatures are shown. The purpose was to see how much variation of temperature measurement with the camera would be caused by different blackbody reference conditions. The larger sensitivity settings (i.e., 50, 100) correspond to observing a larger temperature range on the sphere but likewise correspond to a lower temperature resolution. The lower sensitivity settings (i.e., 10, 20) correspond to observing a small temperature range on the sphere and hence to a high temperature resolution. The temperature scale in these pictures is with white as the highest temperature, yellow the next highest, etc. (in accordance with the color scale at the bottom of the pictures). The highest temperature color observed on the reference blackbody (at the lower left of each figure) actually corresponds to the blackbody temperature. This corresponds to the blackbody case, which actually simulates blackbody conditions. To actually compute the temperature of the different segments shown in Figs. 49 through 57 one must follow the instructions and calibration curves in Ref. 6. Figure 58 was recorded under ambient conditions with aluminum tape over the approximate thermocouple locations (also see Fig. 12b to locate thermocouples 1, 10, 11, and 20). More of the sphere is shown in Figs. 50 and 52 because the sensitivity is 100 and therefore the temperature span of the camera is larger. The lower sensitivity numbers correspond to small temperature ranges, and hence only small portions of the sphere (Figs. 40 and 41) are recorded. The results of these various blackbody temperature settings and camera sensitivity settings are recorded in Table 6. This table shows that the camera measurements and thermocouple measurements are in excellent agreement. The error indication for the camera measurements is a function of the reference temperature, camera calibration, and sensitivity setting. For Table 6 these settings were chosen to measure the temperature of thermocouple location 11 most accurately. The error settings on the other thermocouple locations can be improved upon by using different camera sensitivities and camera gain.

5.0 CONCLUSIONS

From the results of this test, several conclusions can be reached about the quality of the AEDC and DFVLR space simulation facilities and about the nature of chamber hot spots. From the AEDC test, it would appear that for thermal vacuum testing the filtered solar beam did not significantly affect the thermal balance. However, the filtered solar does become important for sensor testing. A comparison between

the results of AEDC and DFVLR (Figs. 13 and 19) would indicate that the divergent solar beam at DFVLR causes slightly higher sphere temperatures at the top of the sphere because the beam flux is slightly greater than one solar constant, whereas AEDC employs a collimated solar beam. From the results obtained without solar simulation (Figs. 24 and 25), a comparison shows the AEDC data to be almost uniformly 6°C higher than the DFVLR results.

The results for the 21°C plate temperature show that, with the solar on, the presence of the plate is noticeable but insignificant. With the solar off, the presence of the 21°C plate has a significant effect on the integral equilibrium temperature. The maximum temperature distribution across the sphere (without solar simulation) was only about 8°C. The presence of a 21°C hot spot on an actual test article, where thermal conduction (in the circumferential direction) would be important, would probably be insignificant with respect to changing the temperature distribution.

The results for the 125°C plate temperature showed a significant effect on the sphere temperature distribution both with and without solar simulation, as well as upon the integral equilibrium temperature. The temperature difference across the sphere when there was no solar simulation was about 26°C.

The results of the Phase III tests with the internal heaters showed the same general trends as the DFVLR theoretical data in Ref. 6. The measured changes in temperature from the initial cold equilibrium conditions are consistently lower than the respective theoretical values because of the radiation losses from the strip heaters. The Phase III results show that the sphere can be used to investigate chamber hot spots which result in a net heat flux of at least 0.25 w or larger for individual segments.

The results for Phase IV showed that the measurements of temperature with the IR camera were in excellent agreement with the thermocouple results. Also, the IR camera indicated, for the black sphere tested, that there was no problem associated with reflected radiation in the 2- to 5-μm wavelength band. It would appear that the IR camera is very useful as a supplementary instrument for obtaining data in thermal vacuum testing. The camera records data remotely and provides a temperature (or radiant flux) map over a broad region of the test article and not just at a few discrete points, as with thermocouples. In addition, the IR camera would appear to be very useful for measuring exhaust plume radiance.

REFERENCES

1. Smith, A. M. and Lee, A. Y. "Analytical Study of a Solar Degradation Model for Thermal Control Materials and Some Ramifications for Accelerated Solar Radiation Testing." AEDC-TR-68-175 (AD675140), September 1968.

2. Mills, D. W., Jr. and Smith, A. M. "Effect of Reflections from CO_2 Cryopanel Deposits on the Thermal Balance of a Test Model in a Space Simulation Chamber." AEDC-TR-69-226 (AD862780), December 1969.

3. Lorenz, A. and Hallmann, Ing. W. "Ergelnissedes Weltraumsemutationstests in der groβ en Simulationskammer des Instituts für Raumsimulation der DFVLR in Wahn." Testdaver 15./16.09 und 01.10.69.

4. Latture, N. C. "DFVLR/AEDC Cooperative Thermal Test." AEDC-TR-71-9 (AD879452), January 1971.

5. Latture, N. C. "DFVLR/AEDC Cooperative Thermal Test II." AEDC-TR-72-54 (AD740899), May 1972.

6. Hallman, W., Kramp, K. and Schmidt, H. P. "Zum Problem der 'Eichkörper' beim Vergleich von Messungen in verschiedenen Weltramsimulationskammern." IB-74/62 (DFVLR).

7. "AGA Thermovision System 680/102B Operating Manual." AGA AKTIEBOLAG-Infrared Instruments, Lidingö, Sweden.